International Journal of Nanomedicine

Dovepress
open access to scientific and medical research

Open Access Full Text Article

ORIGINAL RESEARCH

Combined Biomimetic MOF-RVG15 Nanoformulation Efficient Over BBB for Effective Anti-Glioblastoma in Mice Model

Hao Wu[1,2], Yanhong Liu[2], Liqing Chen[2], Shuangqing Wang[1,2], Chao Liu[2], Heming Zhao[2], Mingji Jin[1,2], Shuangyan Chang[2], Xiuquan Quan[3], Minhu Cui[3], Hongshuang Wan[2,3], Zhonggao Gao[1,2], Wei Huang[2]

[1]Key Laboratory of Natural Medicines of the Changbai Mountain, Ministry of Education, College of Pharmacy, Yanbian University, Yanji, Jilin Province, 133002, People's Republic of China; [2]State Key Laboratory of Bioactive Substance and Function of Natural Medicines, Department of Pharmaceutics, Institute of Materia Medica, Chinese Academy of Medical Sciences and Peking Union Medical College, Beijing, 100050, People's Republic of China; [3]Department of Gastroenterology, Yanbian University Hospital, Yanji, Jilin Province, 133000, People's Republic of China

Correspondence: Zhonggao Gao; Wei Huang, Tel +86 10 63028096; +86 10 63026505, Email zggao@imm.ac.cn; huangwei@imm.ac.cn

Introduction: The blood–brain barrier (BBB) is a key obstacle to the delivery of drugs into the brain. Therefore, it is essential to develop an advanced drug delivery nanoplatform to solve this problem. We previously screened a small rabies virus glycoprotein 15 (RVG_{15}) peptide with 15 amino acids and observed that most of the RVG_{15}-modified nanoparticles entered the brain within 1 h of administration. The high BBB penetrability gives RVG_{15} great potential for brain-targeted drug delivery systems. Moreover, a multifunctional integrated nanoplatform with a high drug-loading capacity, tunable functionality, and controlled drug release is crucial for tumor treatment. Zeolitic imidazolate framework (ZIF-8) is a promising nanodrug delivery system.

Methods: Inspired by the biomimetic concept, we designed RVG_{15}-coated biomimetic ZIF-8 nanoparticles (RVG_{15}-PEG@DTX@ZIF-8) for docetaxel (DTX) delivery to achieve efficient glioblastoma elimination in mice. This bionic nanotherapeutic system was prepared by one-pot encapsulation, followed by coating with RVG_{15}-PEG conjugates. The size, morphology, stability, drug-loading capacity, and release of RVG_{15}-PEG@DTX@ZIF-8 were thoroughly investigated. Additionally, we performed in vitro evaluation, cell uptake capacity, BBB penetration, and anti-migratory ability. We also conducted an in vivo evaluation of the biodistribution and anti-glioma efficacy of this bionic nanotherapeutic system in a mouse mode.

Results: In vitro studies showed that, this bionic nanotherapeutic system exhibited excellent targeting efficiency and safety in HBMECs and C6 cells and high efficiency in crossing the BBB. Furthermore, the nanoparticles cause rapid DTX accumulation in the brain, allowing deeper penetration into glioma tumors. In vivo antitumor assay results indicated that RVG_{15}-PEG@DTX@ZIF-8 significantly inhibited glioma growth and metastasis, thereby improving the survival of tumor-bearing mice.

Conclusion: Our study demonstrates that our bionic nanotherapeutic system using RVG_{15} peptides is a promising and powerful tool for crossing the BBB and treating glioblastoma.

Keywords: glioblastoma, blood–brain barrier, RVG15, biomimetic nanoparticle, zeolitic imidazolate frameworks-8, ZIF-8

Introduction

Glioma, the most common malignant brain tumor, is recognized as an incurable and deadly forms of cancer. According to a report by the International Agency for Research on Cancer, 308,102 new brain tumors diagnoses resulted in 251,329 deaths worldwide in 2020.[1] Glioblastoma (GBM) is the most rapidly progressing subtype of glioma, with a 5-year survival rate of 5.6%.[2,3] Surgery is the primary treatment for GBM.[4–6] However, it is often difficult to achieve complete resection of the tumor while preserving neurological function. Therefore, chemotherapy is crucial in GBM treatment. Several advanced therapeutic drugs, including immune-activating, small molecule targeted, and antibody drugs, have been successful in other malignant tumors.[7–9] Unfortunately, the blood–brain barrier (BBB) and blood–brain–tumor barrier (BBTB) restrict the current drugs from entering

Received: 26 August 2022
Accepted: 1 December 2022
Published: 15 December 2022

the brain for effective GBM treatment.[10] Therefore, many therapeutic agents that are effective against glioma cells in vitro exhibit lower response in vivo.

With advances in nanotechnology and associated molecular biology, numerous strategies have been developed to surpass the BBB and BBTB, including ultrasound or thermal-induced BBB disruption, receptor-mediated transport systems, tight junctions opening, and absorption-mediated transcytosis.[11–13] Nevertheless, these methods allow limited diffusion of therapeutic drugs from blood circulation to the brain. Therefore, it is essential to develop advanced drug delivery strategies for effective GBM treatment. Polypeptides are small molecules consisting of 2–50 amino acids. When a peptide ligand binds to a receptor, a nanocarrier linked to the peptide enters the cell via receptor-mediated endocytosis. Examples of RGD peptides include cyclic RGD peptides (cRGD) or internalized RGD peptides (iRGD).[14–16] Cell-penetrating peptides (CPPs), such as rabies-derived peptides (RDPs), are also of interest because they can transport exogenous molecules to tumor tissue.[17,18] Recently, biomimetic concepts have been integrated into the design of drug delivery systems.[19,20] Rabies virus, a powerful natural invader, has evolved the ability to quickly invade the brain and cause lethal neurological infections in humans.[21] Rabies virus glycoprotein (RVG), which is expressed on the surface of the rabies virus, plays a major role in viral entry and infection by binding to the nicotinic acetylcholine receptor (nAChR) on brain endothelial and neuronal cells.[22,23] Inspired by the function of RVG, we designed a drug delivery system disguised by RVG-derived peptides, which provides brain targeting and penetration functions. RVG_{29} is a 29-amino-acid peptide derived from RVG. It relies on binding to nAChR, which can facilitate different types (nucleic acids, genes, or drugs) of drugs to traverse the BBB and accumulate in the brain.[24,25] Over the past few years, considerable advances have been made in RVG_{29}-mediated targeted therapies for brain diseases.[26–28] In consideration of its high molecular weight, RVG_{29} has been exploited as a ligand, and the increasing nanoparticle size further increases its complexity and cost of the manufacturing. Previous studies have shown that it is more difficult for nanoparticles with larger particle sizes to cross the BBB.[29,30] Based on the above facts, we successfully screened a smaller RVG_{15} peptide with 15 amino acid sequences and found that RVG_{15}-modified nanoparticles had a smaller particle size and higher brain-targeted efficiency. The in vivo biodistribution assay revealed that most of these nanoparticles entered the brain within 1 h of injection. The high and efficient ability to target the brain holds great potential for the clinical transformation of RVG_{15}-based brain-targeted drug delivery systems.

In recent years, nanocarriers have been successfully used as a potential drug delivery system for targeting brain glioma.[31–33] Metallic nanoparticles are emerging as nanocarriers with wide applications in glioma treatment. Some examples include nanoparticles that (i) permeate the blood-brain barrier by using iron oxide nanoparticles,[34] (ii) selectively target glioma with gold nanoparticle-induced radiosensitization,[35] and (iii) promote photodynamic effects with multifunctional silica-based hybrid nanoparticles.[36] Metal organic frameworks (MOFs) are organic–inorganic hybrid materials assembled from coordinated metal ions and organic ligands.[37] Remarkably, MOFs have been demonstrated to be promising nanoplatforms for drug delivery because of their high drug-loading capacity, easy functionalization, tunable pore sizes, and controllable synthesis.[38–41] Zeolitic imidazolate framework-8 (ZIF-8) constitute a subcategory of MOFs that are formed by the self-assembly of zinc ions and 2-methylimidazole (2-MIM).[42] In addition to the inherent advantages of MOFs, ZIF-8 quickly degrades in the weakly acidic microenvironment due to protonation, which allows pH-controllable release of the encapsulated drugs in the endosomal and/or lysosomal environment of tumor cells.[43] This pH-sensitive degradation makes ZIF-8 nanoparticles a promising nanodrug delivery system for tumor treatment.[44–47]

Docetaxel (DTX) is a broad-spectrum antineoplastic drug, derived from paclitaxel, which was developed by Planck Le Rhone. As a first-line strategy against various types of cancers, DTX is used clinically for the treatment of breast, ovarian, non-small cell lung, and prostate cancers.[48] DTX stabilizes microtubules, blocks angiogenesis, and inhibits tumor cell mitosis.[49] However, owing to its poor water solubility and low BBB penetration, promising therapeutic effects have not been achieved of glioma treatment.[50] Therefore, developing a drug delivery system to deliver DTX to gliomas across the BBB is of great clinical value.

In this study, we developed a RVG_{15}-coated biomimetic ZIF-8 nanoparticle (RVG_{15}-PEG@DTX@ZIF-8) was rationally designed to deliver DTX for efficient GBM elimination. We characterized the size, morphology, stability, drug-loading capacity, and drug release of RVG_{15}-PEG@DTX@ZIF-8 using multiple technologies. Additionally, we studied the in vitro antitumor effect, cell uptake capacity, BBB penetration, anti-migratory ability, and tissue distribution of this bionic nanotherapeutic system. Finally, the therapeutic efficacy and biocompatibility were verified using a murine orthotopic GBM model.

Our bionic nanotherapeutic system effectively overcomes the BBB and BBTB and enters the mouse brain by specific binding to nAChR on brain endothelial cells and neuronal cells. After entering glioma tumors, precise pH-sensitive DTX release was achieved via pH-responsive degradation in the endosomal and/or lysosomal environment of tumor cells. Therefore, our RVG_{15}-mediated bionic nanosystem is a promising tool for GBM treatment.

Materials and Methods

Synthesis and Characterization of Carboxylated Polyethylene Glycol 2000 Modified with RVG_{15} (RVG_{15}-PEG_{2000}-COOH)

RVG_{15}-PEG_{2000}-COOH (Ruixi, China) was synthesized by conjugating the cysteine residue of RVG_{15}-Cys to COOH-PEG_{2000}- Mal (Ruixi, China) according to a previously reported method.[51] RVG_{15}-Cys and COOH-PEG_{2000}-Mal (at a molar ratio of 1.5:1) were dissolved in HEPEs buffer (pH 8.0) in a nitrogen atmosphere for protection. The reaction was performed with gentle stirring at ambient temperature for 16 h. The resulting reaction mixture was separated by dialysis (MWCO 2500Da) for 24 h against free RVG_{15}. The final product was obtained via cryodesiccation. The synthesis of RVG_{15}-PEG_{2000}-COOH was confirmed using ^{1}H NMR spectroscopy (500 MHz, Varian Medical Systems, Inc., Palo Alto, CA, USA). This was further verified using matrix-assisted laser desorption/ionization time-of-flight mass spectrometry (MALDI-TOF-MS) (4800 Plus, Applied Biosystems Inc., Waltham, MA, USA). For MALDI-TOF-MS analysis, 3-indoleacetic acid (IAA) was used as the detection matrix.

Preparation and Characterization of DTX@ZIF-8 with or Without RVG_{15} Modification

DTX@ZIF-8 nanoparticles were prepared using a simple one-pot synthesis as described in previous reports, with some modifications.[52] In detail, 5 mg of DTX (Meilun, China) and 80 mg of $Zn(NO_3)_2{\cdot}6H_2O$ (Macklin, China) were dissolved in 3 mL of DMSO. The mixture was then stirred for 30 min. Thereafter, 6 mL of an aqueous solution containing 800 mg of 2-methylimidazole (Macklin, China) was added dropwise while stirring. The resulting solution was stirred for 30 min. Finally, DTX@ZIF-8 nanoparticles were obtained by centrifugation (18,000 rcf, 15 min) and washed three times with methanol. DTX@ZIF-8 nanoparticles with RVG_{15} modification (RVG_{15}-PEG@DTX@ZIF-8) were prepared by coating RVG_{15}-PEG_{2000}-COOH on the surface of the DTX@ZIF-8 nanoparticles via electrostatic interactions. RVG_{15}-PEG_{2000}-COOH conjugates were dissolved in water and added to an aqueous solution containing DTX@ZIF-8 nanoparticles (quality ratio = 1:5). The mixture was stirred gently in the dark at 25 °C for 12 h, then was centrifuged at 10,000 rcf for 15 min, and washed three times with water. Blank ZIF-8 was prepared under the same conditions but without the addition of DTX.

The mean particle size, polydispersity index, and zeta potential of the as-prepared nanoparticles were determined by dynamic light scattering (DLS) and electrophoretic light scattering (Zetasizer Nano ZS90; Malvern Instruments Ltd., UK). The morphology of the nanoparticles was characterized by transmission electron microscopy (JEM-1400PLUS; JEOL Ltd., Tokyo, Japan) at an acceleration voltage of 200 kV. Morphological analysis was conducted using a scanning electron microscope (LV-6380; JEOL, Sweden) and elemental mapping was performed using energy dispersive X-ray spectroscopy (EDX). X-ray diffraction analysis of the nanoparticles was performed using a Rigaku D/MAX2550 diffractometer with CuKα radiation at 40 kV and 200 mA at a scanning rate of 0.4° min^{-1}. The stability of the as-prepared nanoparticles was investigated using changes in the particle size in phosphate buffer saline (PBS, 0.01 M, pH 7.4), which were characterized by DLS.

The encapsulation efficiency (EE%) and drug-loading capacity (DL%) of DTX were determined using HPLC (SHIMADZU SPD-20A, Japan). The EE% and DL% of DTX in the as-prepared nanoparticles were calculated using the following equations:

$$EE\% = (\text{weight of encapsulated drug})/(\text{weight of total drug}) \times 100\%$$

$$DL\% = (\text{weight of encapsulated drug})/(\text{weight of total drug and nanoparticles}) \times 100\%$$

To prepare coumarin 6 (Cou-6)-or new indocyanine green (IR-820)-labeled MOFs, DTX in DTX@ZIF-8 and RVG_{15}-PEG@DTX@ZIF-8 were replaced by Cou-6 or IR-820. The other steps were similar in implementation to those described above.

In vitro Release of RVG_{15}-PEG@DTX@ZIF-8

The in vitro release profile of DTX was studied in PBS (pH 7.4, 6.8, and 5.5) containing 0.5% (v/v) Tween 80, using the dialysis diffusion method. One milliliter of RVG_{15}-PEG@DTX@ZIF-8 at a DTX concentration of 2 mg/mL was added to dialysis bags (MWCO, 12000Da). The bags were immersed in 20 mL of PBS at different pH values and shaken at 100 rpm and 37 °C. Samples (0.5 mL) were obtained at each time interval, and an equal amount of fresh release medium was immediately added. The collected samples were centrifuged (18000 rcf, 10 min), and the supernatant was analyzed for DTX content using a previously established HPLC method.[53] Finally, the cumulative release of DTX was calculated and an in vitro release curve was plotted.

Cell Line and Cell Culture

Rat C6 glioma cells, human brain microvascular endothelial cells (HBMECs) and 4T1 mouse mammary breast tumor cell were obtained from the Cell Culture Center of the Institute of Basic Medical Sciences at the Chinese Academy of Medical Sciences (CAMS, China). Rat C6 and 4T1 cells were cultured in Roswell Park memorial institute-1640 (RPMI-1640) (Gibco, USA) medium supplemented with 10% (v/v) fetal bovine serum (FBS) (Gibco, USA) and 1% (v/v) penicillin-streptomycin (Pen-Strep) (Gibco, USA). HBMECs were cultured in Dulbecco's modified Eagle's medium (DMEM) (Gibco, USA) supplemented with 10% FBS and 1% Pen-Strep. The cells were cultured in a humidified atmosphere at 37 °C and 5% CO_2.

The Examination of Drug Uptake Using Different Cell Types

The green fluorescent probe coumarin-6-labeled MOF nanoparticles with or without modified RVG_{15} (RVG_{15}-PEG@Cou-6@ZIF-8 and Cou-6@ZIF-8) were constructed to visualize the cellular uptake and localization of nanoparticles in both HBMECs and C6 cells. HBMECs and C6 cells were seeded on round glass coverslips at the bottom of 12-well plates at a density of 15×10^4 cells/well for 24 h of culture at 37 °C and 5% CO_2. The cell culture medium was then removed, and a fresh medium containing free Cou-6, Cou-6@ZIF-8, or RVG_{15}-PEG@Cou-6 @ZIF-8 nanoparticles at a Cou-6 concentration of 5 μg/mL was added. After incubation for 15, 60, 120, and 240 min at 37 °C, respectively, the cells were washed three times with cold PBS and fixed with 4% paraformaldehyde in PBS for 15 min. The cell nuclei were stained with DAPI (Solarbio, China). for 10 min. Finally, the cells were observed and analyzed by confocal laser scanning microscopy (CLSM, TCS SP2; Leica, Germany).

To quantitatively evaluate the cellular uptake efficiency of the prepared nanoparticles, flow cytometry analysis was performed to measure the fluorescence intensity of the stained cells. Briefly, HBMECs or C6 cells were seeded in 6-well plates at a density of 15×10^4 cells/well for 24 h of culture under 37 °C and 5% CO_2. Next, the cells were incubated with a fresh medium containing free Cou-6, Cou-6@ZIF-8, or RVG_{15}-PEG@Cou-6@ZIF-8 nanoparticles for 15, 60, 120, and 240 min at 37 °C, respectively. The final concentration of Cou-6 was 1 μg/mL. The cells were washed three times with cold PBS, collected via trypsinization and centrifugation, and resuspended in fresh PBS. The fluorescence intensity of the cells was measured by flow cytometry (Becton Dickinson, Franklin Lake, NJ, USA).

Uptake Mechanism Study of RVG_{15}-PEG@DTX@ZIF-8

To identify the cellular internalization pathways of the as-prepared nanoparticles in C6 cells, the cells were first cultured with different specific endocytic inhibitors respectively, including RPMI 1640 (control), methyl-β-cyclodextrin (5 mg/mL), sodium azide (3 mg/mL), chlorpromazine hydrochloride (10 μg/mL), and colchicine (4 μg/mL), for 1 h at 37 °C. Subsequently, the cells were incubated with RVG_{15}-PEG@Cou-6@ZIF-8 nanoparticles for 2 h. The cells were then washed three times with PBS, trypsinized, collected, and analyzed by flow cytometry. To investigate whether nanoparticles exhibit nAChR receptor-mediated endocytosis, excess RVG_{15} was incubated with HBMECs and C6 cells for 1 h, respectively, and were then incubated with RVG_{15}-PEG@Cou-6@ZIF-8 (at a Cou-6 concentration of 5 μg/mL) for 240

min. 4T1 cells with low nAChR-expression were used as controls. The cells were washed three times with cold PBS and fixed with 4% paraformaldehyde in PBS for 15 min. The cell nuclei were stained with DAPI for 10 min. Finally, the cells were observed and analyzed using CLSM.

C6 and HBMECs Cells Viability Assay

The in vitro cytotoxicity of the prepared nanoparticles on C6 cells was evaluated using a CCK-8 (Dojindo, Japan) assay. C6 cells were plated into 96-well plates at a density of 5×10^3 cells/well and were cultured for 24 h. Cells were then treated with fresh medium containing serial concentrations of free DTX, DTX@ZIF-8, and RVG_{15}-PEG@DTX@ZIF-8 for an additional 24 or 48 h of culture. CCK-8 reagent was added to each well and the cells were incubated for another 2 h. Finally, the absorbance of the plates was measured at 450 nm using a Synergy H1 Microplate Reader (BioTek, Dallas, TX, USA). Blank and negative controls were simultaneously implemented, and six replicates were performed for each sample.

Moreover, the CCK-8 assay was performed to investigate the in vitro biocompatibility of blank ZIF-8 nanoparticles on both HBMECs and C6 cells. The operational processes were similar to those of the in vitro cytotoxicity assays. Cell viability was calculated as follows:

$$\text{Cell viability } (\%) = (\text{OD test} - \text{OD blank})/(\text{OD control} - \text{OD blank}) \times 100\%$$

C6 Cell Apoptosis Assay

The anti-glioma activity of the as-prepared nanoparticles was quantitatively analyzed using an annexin V-FITC/PI double staining assay. C6 cells were plated into 12-well plates at a density of 15×10^4 cells/well and were grown for 24 h. The cells were treated for 24 h with blank ZIF-8, free DTX, DTX@ZIF-8, or RVG_{15}-PEG@DTX@ZIF-8 (at a DTX concentration of 0.5 μg/mL), with the culture medium as a control. The cells were collected via trypsinization and centrifugation and then resuspended in binding buffer. Finally, 5 μL of annexin V-fluorescein isothiocyanate (FITC) and 5 μL propidium iodide (PI) were added to the cells. The percentage of apoptotic cells was determined using flow cytometry. For qualitative analysis, the cells were fixed with 4% paraformaldehyde at 37 °C for 15 min, stained with Hoechst stain at 37 °C for 15 min, and then washed three times with cold PBS. The stained cells were examined by CLSM.

In vitro Wound-Healing Assay

In this assay, the motility and migratory ability of tumor cells after treatment with different formulations were evaluated. C6 cells were plated in 6-well plates and cultured until they formed a monolayer. A scratch wound was created in the middle of the well using a sterile 200-μL pipette tip. The cells were washed with PBS to remove detached cells. The cells were treated with free DTX, DTX@ZIF-8, or RVG_{15}-PEG@DTX@ZIF-8 at a DTX concentration of 1 μg/mL. Fresh medium was used as control. Migrating cells in the wound area were observed and imaged at 0, 12, and 24 h using an inverted light microscope (Olympus, Hamburg, Germany).

In vitro Drug Penetration in the Blood–Brain Barrier Model

The in vitro BBB model was established using a Transwell system according to previously reported methods.[54,55] Generally, HBMECs were placed into the upper side of 12-well Transwell inserts (0.4 μm pore size; Corning Co., Corning, NY, USA) at a density of 2×10^5 cells/insert, and the culture medium was replaced every 2 d. Potential BBB models were evaluated by measuring the transepithelial electrical resistance (TEER) using a TEER instrument (Millicell-ERS-2; Millipore, USA). Monolayers were selected for BBB penetration studies when the TEER value exceeded 200 $\Omega\cdot cm^2$.[56]

To investigate the ability of the as-prepared nanoparticles to cross the BBB, C6 cells were seeded in the lower chamber at a density of 1×10^5 cells/well and were incubated overnight. Cou-6, Cou-6@ZIF-8, and RVG_{15}-PEG@Cou-6@ZIF-8 were added to HBMECs monolayers on the upper side of the inserts. The cells were then co-cultured for 3 h. After incubation, C6 cells in the lower chamber were washed three times with cold PBS and fixed with 4% paraformaldehyde for 15 min. C6 cell nuclei were stained with DAPI, and the BBB penetration and targeting ability

of RVG_{15}-PEG@Cou-6@ZIF-8 were analyzed using CLSM. For quantitative analysis, the fluorescence intensity of C6 cells was measured by flow cytometry using the same experimental procedures described in the "The examination of Drug uptake using different cell" section above.

Establishment of Glioma Models

Six-week-old male ICR mice (22 ± 2 g) were purchased from Vital River Laboratory Animal Technology Co., Ltd. (Beijing, China). All animal experiments were conducted in accordance with protocols approved by the Laboratory Animal Ethics Committee of the Institute of Materia Medica in CAMS and PUMC. The operational process followed the national and institutional principles and protocols for the care and use of experimental animals.

Based on our previous study, an orthotopic glioma-bearing mouse model was established. Briefly, 2×10^5 C6 cells were suspended in 4 μL PBS and were slowly injected into the brains of anesthetized ICR mice (1.8 mm right-lateral to the bregma and 3.0 mm deep from the dura) using a stereotaxic instrument. The burr hole was sealed with bone wax and the scalp incision was sutured. The sham-operated group was operated in the same way as above, with blank PBS replacing the PBS containing C6 cells. Glioma-bearing mice were raised under standard conditions for 1 week and were used for subsequent experiments.

In vivo Nanosystem Biodistribution

The biological distribution and brain accumulation of systemically administered nanoparticles were investigated using an IVIS Spectrum CT in vivo imaging system. MOF nanoparticles with or without modified RVG_{15} were labeled with the new indocyanine green (IR-820) for easy observation in vivo. Orthotopic glioma-bearing mice were randomly divided into three groups (n = 3), which were injected with 200 μL free IR-820, IR-820@ZIF-8, or RVG_{15}-PEG@IR-820@ZIF-8 (2 mg/kg of IR-820), respectively, via the tail vein. Subsequently, fluorescent images of the mice were acquired at predetermined times post-injection (1, 4, 8, and 24 h) using an in vivo imaging system (Caliper Life Sciences Inc., Mountain View, CA, USA). To further analyze the distribution of the different nanoparticle formulations in the organs and tumors, the mice were sacrificed, and the main organs (heart, liver, spleen, lung, and kidney) and tumor-bearing brains were collected at 24 h. Fluorescent images were obtained using an in vivo imaging system, and the intensities were analyzed using Living Image software (version 4.3.1; Caliper Life Sciences Inc.).

In vivo Glioma-Bearing Brain Biodistribution

Fresh frozen slices of the brain were stained and utilized to investigate BBB penetration and distribution of the as-prepared nanoparticles in gliomas. Orthotopic glioma-bearing mice were randomly divided into two groups and were intravenously injected with free Cou-6 or RVG_{15}-PEG@Cou-6@ZIF-8 (1.5 mg/kg of Cou-6). Three hours after the injection, the mice were anesthetized and heart perfusion was conducted with saline and 4% paraformaldehyde. The brains were collected, and frozen sections of 10 mm thickness were prepared. The sections were stained with DAPI and observed using CLSM to explore fluorescence distribution at the glioma site.

In vitro Anti-Glioma Efficacy

Seven days after tumor implantation, orthotopic glioma-bearing mice were randomly divided into four groups (n = 6) and treated with saline, free DTX, DTX@ZIF-8, or RVG_{15}-PEG@DTX@ZIF-8 at a dose of 5 mg/kg of DTX via tail vein injection. Mice treated with saline were used as the negative controls. The treatments were repeated every 3 days for 5 times. To evaluate the volume of glioma, the anti-glioma effects were evaluated using magnetic resonance imaging (MRI; PharmaScan 70/16 US; Bruker, Germany) at the conclusion of the treatment. Glioma volume was calculated as the sum of all areas with tumors assessed by MRI tomography × thickness of each layer. In addition, the body weights of the mice were monitored to analyze biosafety. Three days after the final treatment, the mice were sacrificed and the brains and main organs (kidneys, hearts, lungs, livers, and spleens) were collected. TUNEL assays were performed to detect apoptosis in glioma cells. To evaluate the antimetastatic efficacy, the major organs (heart, liver, spleen, lung, and kidney) were fixed in 4% paraformaldehyde, embedded in paraffin, and stained with hematoxylin and eosin for biocompatibility and tissue cytotoxicity analysis. Finally, blood biochemical analysis was performed for bio-safety evaluation, including

creatinine (CRE), alanine aminotransferase (ALT), serum aspartate aminotransferase (AST), and blood urea nitrogen (BUN).

Survival times of the other mice (n = 10) of four groups. Survival curves were plotted using GraphPad Prism software (version 8.0; GraphPad Software Inc., La Jolla, CA, USA).

Statistical Analysis

All data are presented as mean ± standard deviation (SD). Statistical data comparisons among groups were performed by Student's *t*-test or one-way ANOVA using the SPSS software (version 23.0, SPSS, Inc., Chicago, IL, USA). *P < 0.05, **P < 0.01 and ***P < 0.001 were considered to be statistically significant.

Results and Discussion

Synthesis and Characterization of Carboxylated Polyethylene Glycol 2000 Modified with RVG_{15} (RVG_{15}-PEG_{2000}-COOH)

First, as illustrated in Figure 1A, COOH-PEG_{2000}-RVG_{15} conjugates were constructed via an addition reaction between the terminal sulfhydryl group of the RVG_{15} peptide and maleimide of COOH-PEG_{2000}-Mal. The ^{1}H NMR spectra of COOH-PEG_{2000}-Mal and COOH-PEG_{2000}-RVG_{15} are presented in Figures 1B and 1C, respectively. Compared to that of Mal-PEG_{2000}-COOH, the characteristic peak representing the double bond of maleimide (6.74 ppm) disappeared after conjugation with RVG_{15}, indicating the successful synthesis of COOH-PEG_{2000}-RVG_{15}. The MALDI-TOF-MS spectra are shown in Figure 1D–F. The average molecular weight (MW) of RVG_{15}, COOH-PEG_{2000}-Mal, and COOH-PEG_{2000}-RVG_{15} were approximately 1980, 2000, and 3980 Da, respectively. The average MW of COOH-PEG_{2000}-RVG_{15} was consistent with the theoretically calculated MW, which further indicated successful synthesis of the target product.

Preparation and Characterization of DTX@ZIF-8 with or Without RVG_{15} Modification

DTX@ZIF-8 nanoparticles were successfully prepared using a simple one-pot synthesis process. Then, the RVG_{15}-PEG_{2000}-COOH shells with brain-targeted properties were coated on the surfaces of DTX@ZIF-8 to obtain RVG_{15}-PEG@DTX@ZIF-8 nanoparticles. The RVG_{15}-PEG_{2000}-COOH conjugates possessed negatively charged carboxyl groups, which interacted with Zn^{2+} ions, thereby enabling successful coating. After intravenous injection, the RVG_{15} shell acted as a smart brain-targeted "guider", thereby endowing the nanoplatform with the ability to rapidly penetrate the BBB and enter the tumor tissue.

The average particle size and surface zeta potential were characterized using DLS analysis. As illustrated in Figure 2A, the average particle size of as-prepared DTX@ZIF-8 and RVG_{15}-PEG@DTX@ZIF-8 nanoparticles were 95±4 nm and 127±3 nm, respectively, with a surface zeta potential of 26.7±0.4 mV and 4.8±0.3 mV, respectively (Figure 2B). Compared with that of the unmodified nanoparticles, the particle size of the RVG_{15}-modified nanoparticles increased slightly owing to the RVG_{15}-PEG_{2000}-COOH coating on DTX@ZIF-8. Notably, the surface zeta potential of the nanoparticles strongly decreased after successful coating with the RVG_{15}-PEG_{2000}-COOH conjugates. The zeta potential is shown to be positively charged because the ZIF-8 nanoparticles expose a large amount of positively charged zinc ions. When RVG_{15}-PEG-COOH is coated on the ZIF-8 surface, the positive charge is neutralized, while PEG shields the ZIF-8 surface charge, so it leads to the decrease of zeta potential. As Furthermore, transmission electron microscopy (TEM) images showed that DTX@ZIF-8 possessed a homogeneous rhombic dodecahedral morphology with sharp edges, truncated corners, and a narrow size distribution (Figure 2D). In contrast, RVG_{15}-PEG@DTX@ZIF-8 nanoparticles displayed a distinct core-shell structure compared to DTX@ZIF-8, which verified the successful coating of the RVG_{15}-PEG_{2000}-COOH shell on the surface of the nanoparticles. As shown in Figures S1A and B, the results showed that RVG_{15}-PEG@DTX@ZIF-8 incubated in PBS (pH 6.8) for 24 h showed weak cleavage of the nanoparticle surface, but the nanoparticles were not significantly disrupted. In contrast, after 24h incubation at pH 5.5, the RVG_{15}-PEG@DTX@ZIF-8 nanoparticles were completely disrupted, aggregated and the drug precipitated. As shown in Figures S1C and D, RVG_{15}-PEG@DTX@ZIF-8 particle size increased to 140±4 nm and 278±3 nm after 24

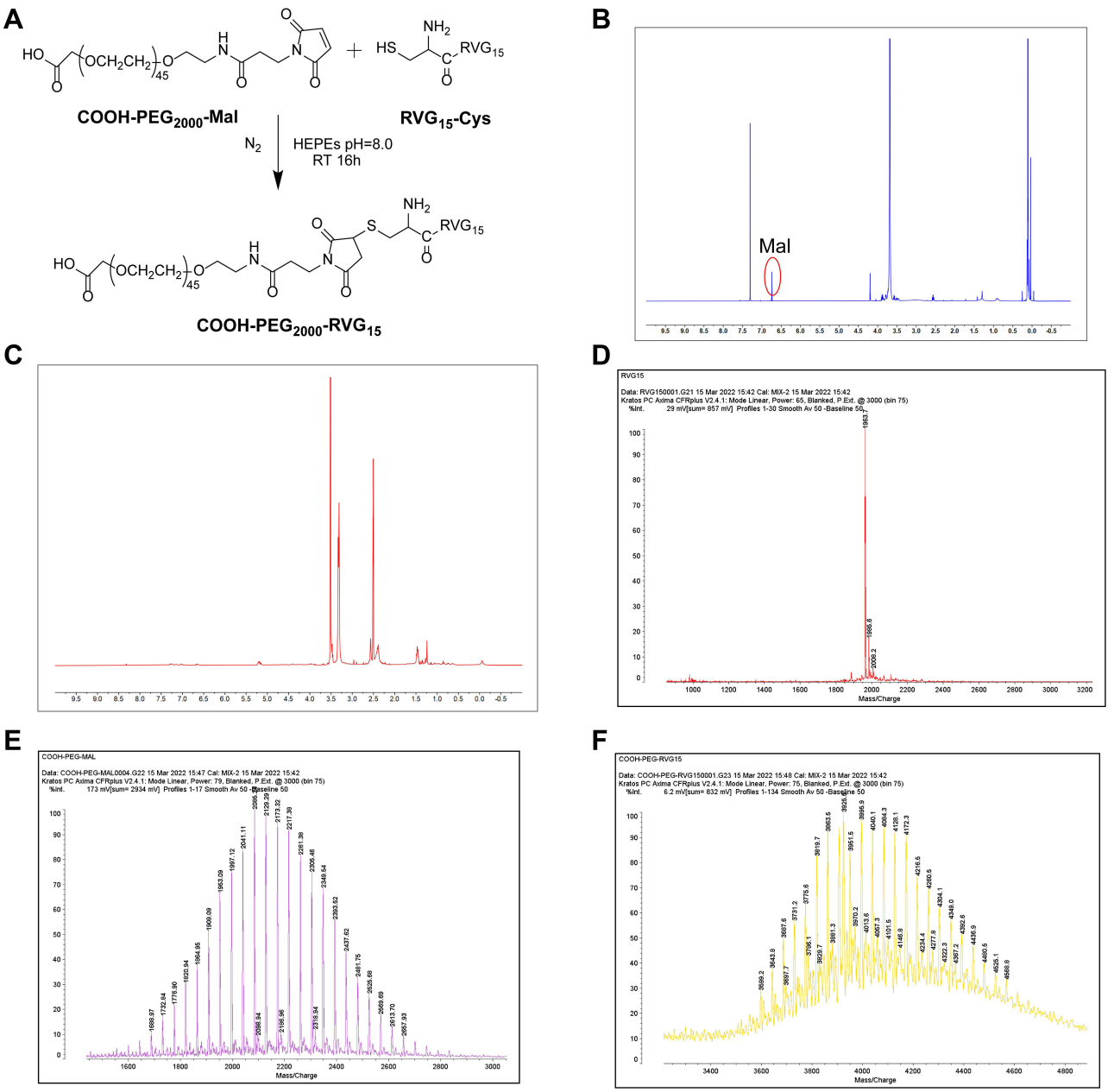

Figure 1 Synthesis and characterization of COOH-PEG$_{2000}$-RVG$_{15}$. (**A**) Synthesis route of COOH-PEG$_{2000}$-RVG$_{15}$. (**B**) ^{1}H NMR spectra of COOH-PEG$_{2000}$-Mal. (**C**) ^{1}H NMR spectra of COOH-PEG$_{2000}$-RVG$_{15}$. (**D**) MALDI-TOF-MS spectra of RVG$_{15}$-Cys. (**E**) MALDI-TOF-MS spectra of COOH-PEG$_{2000}$-Mal. (**F**) MALDI-TOF-MS spectra of COOH-PEG$_{2000}$- RVG$_{15}$.

Abbreviation: ^{1}H NMR spectra, proton nuclear magnetic resonance spectroscopy. MALDI-TOF-MS spectra, matrix-assisted laser desorption/ionization time-of-flight mass spectrometry.

h incubation in PBS buffer at pH 6.8 and 5.5, respectively. Next, scanning electron microscopy was conducted to examine the nanoparticles. As shown in Figure 2E, the as-obtained RVG$_{15}$-PEG@DTX@ZIF-8 had an apparent core-shell structure and smoother surface than DTX@ZIF-8, which is similar to the TEM observation. As shown in the EDX spectrum in Figure S2, the presence of elemental sulfur on the nanoparticle surface was confirmed, attributed to elemental sulfur in RVG$_{15}$-PEG-COOH, thus demonstrating that RVG$_{15}$-PEG-COOH was coated on the surface of DTX@ZIF-8.

Powder X-ray diffraction measurements were performed to determine the crystal structures. As shown in Figure 2C, the diffraction pattern of ZIF-8 coincided with that of the blank ZIF-8 crystal structure. Moreover, the crystal structures of

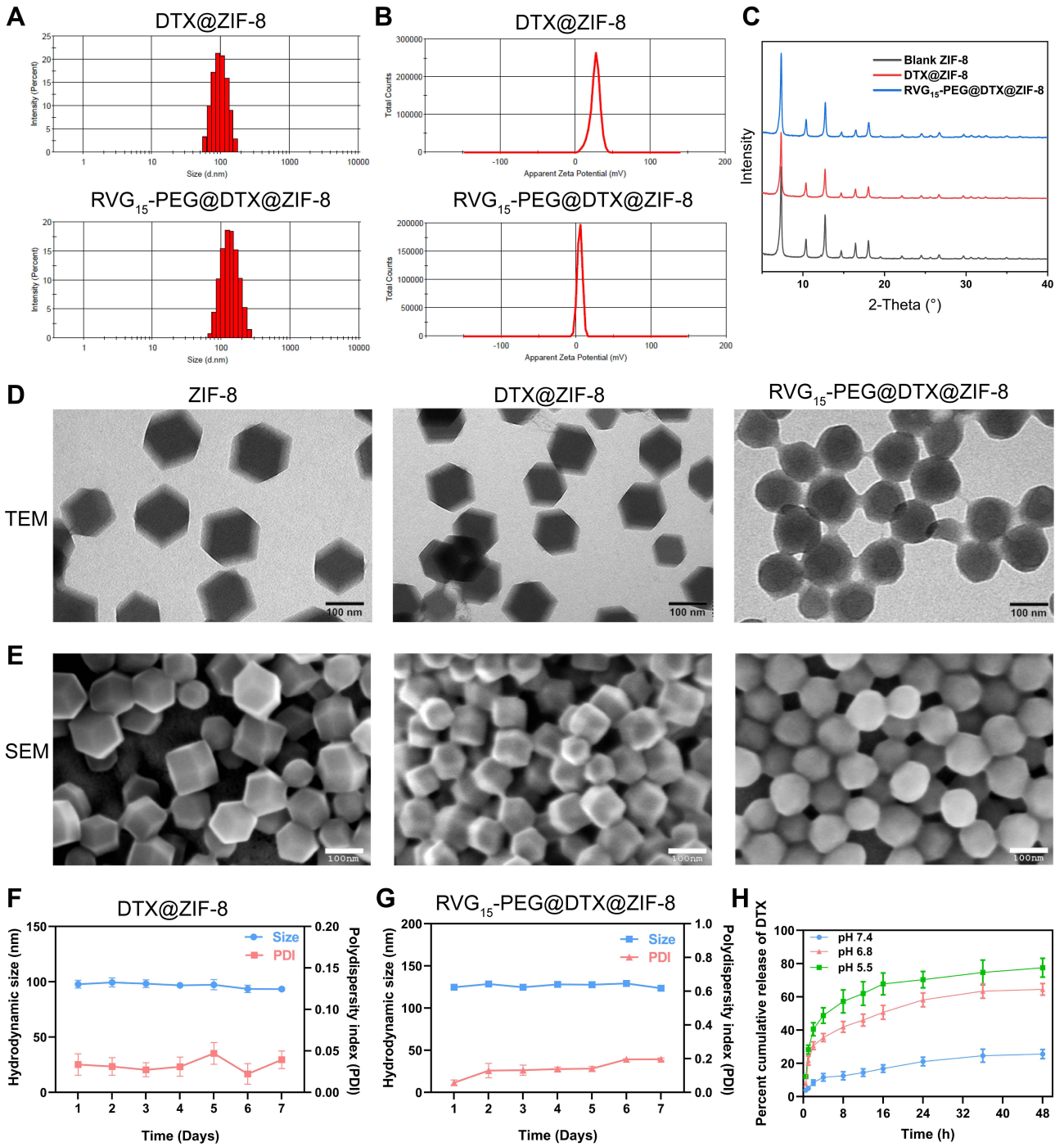

Figure 2 Characterizations of DTX@ZIF-8 and RVG_{15}-PEG@DTX@ZIF-8. (**A**) Size distribution of DTX@ZIF-8 and RVG_{15}-PEG@DTX@ZIF-8 by dynamic light-scattering analysis. (**B**) Zeta potential distribution of DTX@ZIF-8 and RVG_{15}-PEG@DTX@ZIF-8. (**C**) X-ray diffraction patterns of ZIF-8, DTX@ZIF-8, and RVG_{15}-PEG@DTX@ZIF-8. (**D**) Transmission electron microscopy images of ZIF-8, DTX@ZIF-8, and RVG_{15}-PEG@DTX@ZIF-8. (scale bar = 100 nm). (**E**) Scanning electron microscopy images of ZIF-8, DTX@ZIF-8, and RVG_{15}-PEG@DTX@ZIF-8. (scale bar = 100 nm). (**F**) The size stability and zeta potential stability of DTX@ZIF-8 for 7 days. (**G**) The size stability and zeta potential stability of RVG_{15}-PEG@DTX@ZIF-8 for 7 days. (**H**) The pH-responsive release of DTX from RVG_{15}-PEG@DTX@ZIF-8 in a different buffer of pH 5.5, 6.8, and 7.4.

DTX@ZIF-8 and RVG_{15}-PEG@DTX@ZIF-8 were almost the same as that of ZIF-8, indicating that RVG_{15}-PEG_{2000}-COOH coating or drug encapsulation hardly had a strong influence on the structure of the ZIF-8 hosts. In addition, the EE% and DL% of DTX@ZIF-8 and RVG_{15}-PEG@DTX@ZIF-8 were determined by HPLC. RVG_{15} modification did not affect the drug-loading or encapsulation efficiency of the nanoparticles. The EE% and DL% of DTX@ZIF-8 were 84.8±0.5% and 14.4±0.4%,

respectively, which were similar to those of RVG_{15}-PEG@DTX@ZIF-8. The ability of ZIF-8 to encapsulate drugs depends on the chemical structure of the drug, especially the presence of negatively charged groups such as hydroxyl, carboxyl, and sulfonic acid groups. Negatively charged groups can strongly interact with positively charged zinc ions via electrostatic interactions, thus contributing to more drug encapsulation.[57] Docetaxel has carboxyl and hydroxyl groups that can interact with zinc ions. Stirring for 30 min with followed by dimethylimidazole addition caused more DTX encapsulation. Meanwhile, in the water/DMSO system, more DTX was encapsulated than in methanol or water.[52] The above results show that DTX can be efficiently loaded into the nanoparticles. Furthermore, the stability of DTX@ZIF-8 and RVG_{15}-PEG@DTX@ZIF-8 in water was evaluated after storage for 7 d at 4 °C. Figure 2F and G show that the size and polydispersity index of these nanoparticles showed negligible changes, implying good stability. RVG_{15}-PEG@DTX@ZIF-8 with good stability would have a long circulation period in vivo, which would ultimately lead to an increase in drug accumulation in the tumor tissue.

In vitro Release of RVG_{15}-PEG@DTX@ZIF-8

To investigate the pH sensitivity of the formulation, the drug release ability of RVG_{15}-PEG@DTX@ZIF-8 in PBS buffers of different pH was determined (Figure 2H). The results showed that the release rate of DTX from RVG_{15}-PEG@DTX@ZIF-8 in the buffer solution (pH 7.4) was extremely slow, only 25.6% after 48 h. This result indicated that the formulation was relatively stable under neutral physiological conditions and could maintain its structure in the blood and normal tissues, ensuring effective encapsulation of DTX and avoiding damage to the organism due to the early release of the drug. The release rate of DTX increased significantly when the pH of the PBS buffer was decreased from 7.4 to 6.8 or 5.5 (simulating the acidity of the tumor microenvironment and nuclear endosomes/lysosomes, respectively), with a cumulative 48 h release of 64.6% and 77.5%, respectively. This result indicates that RVG_{15}-PEG@DTX@ZIF-8 is unstable under acidic conditions, and after reaching the tumor site and entering the cell, it can disintegrate in a slightly acidic environment, effectively releasing DTX and exerting its drug effect to achieve a specific and controlled release of the loaded drug at the tumor site.

The Examination of Drug Uptake Using Different Cell Types

Given the crucial role of efficient cellular internalization in antitumor activity, the cellular uptake efficiency of the as-prepared nanoparticles by HBMECs and C6 cells, which respectively represented the BBB and glioma tumor, was investigated. The green fluorescent probe coumarin-6 was used to replace DTX to prepare Cou-6@ZIF-8 and RVG_{15}-PEG@Cou-6@ZIF-8. The uptake results of laser scanning confocal microscopy analysis for HBMECs and C6 cells are shown in Figures 3A and 4A, respectively. Cell nuclei were stained with DAPI for blue fluorescence signals. The fluorescence signals of free Cou-6 and Cou-6@ZIF-8 were weak in both HBMECs and C6 cells. In contrast, RVG_{15}-PEG@Cou-6@ZIF-8 showed green fluorescence after incubation for 30 min. Moreover, the increased intensity of the green fluorescence signals with extended incubation times of 60, 120, and 240 min confirmed a time-dependent trend in the cell internalization of RVG_{15}-modified nanoparticles. This result suggests that RVG_{15}-modified nanoparticles can rapidly and easily enter cells, including HBMECs and C6 cells. The remarkable enhancement of cellular uptake exhibited by RVG_{15}-PEG@Cou-6@ZIF-8 was ascribed to the specific binding between RVG_{15} and overexpressed nAChR receptors in the cells. Quantitative analysis of the flow cytometry assay displayed results similar to those of CLSM analysis. RVG_{15}-PEG@Cou-6@ZIF-8 exhibited the highest cellular uptake efficiency in both HBMECs and C6 cells, approximately 1.5-fold higher than that of Cou-6@ZIF-8 and nearly 5.4-fold higher than that of free Cou-6 in HBMEC cells, as well as 1.9-fold and 3.4-fold in C6 cells (Figures 3B and C and 4B and C). Figures 3D and E and 4D and E also show the time-dependent uptake of RVG_{15}-PEG@Cou-6@ZIF-8 in both HBMECs and C6 cells. All the above results demonstrate the enhanced cellular uptake of RVG_{15}-PEG@Cou-6@ZIF-8 nanoparticles, thus laying a solid foundation for in vivo applications.

Uptake Mechanism Study of RVG_{15}-PEG@DTX@ZIF-8

In a subsequent study, the cellular uptake mechanism of RVG_{15}-modified nanoparticles was investigated in C6 glioma cells in the presence of four endocytosis inhibitors: a caveolae-mediated endocytosis inhibitor (methyl-beta-cyclodextrin, M-β-CD), an energy-mediated endocytosis inhibitor (sodium azide), a clathrin-mediated endocytosis inhibitor (chlorpromazine hydrochloride, CPZ), and a microtubule protein inhibitor (colchicine, Col).[58] As shown in Figure 4F, M-β-CD significantly suppressed the cellular uptake of RVG_{15}-PEG@Cou-6@ZIF-8, with a relatively reduced fluorescence

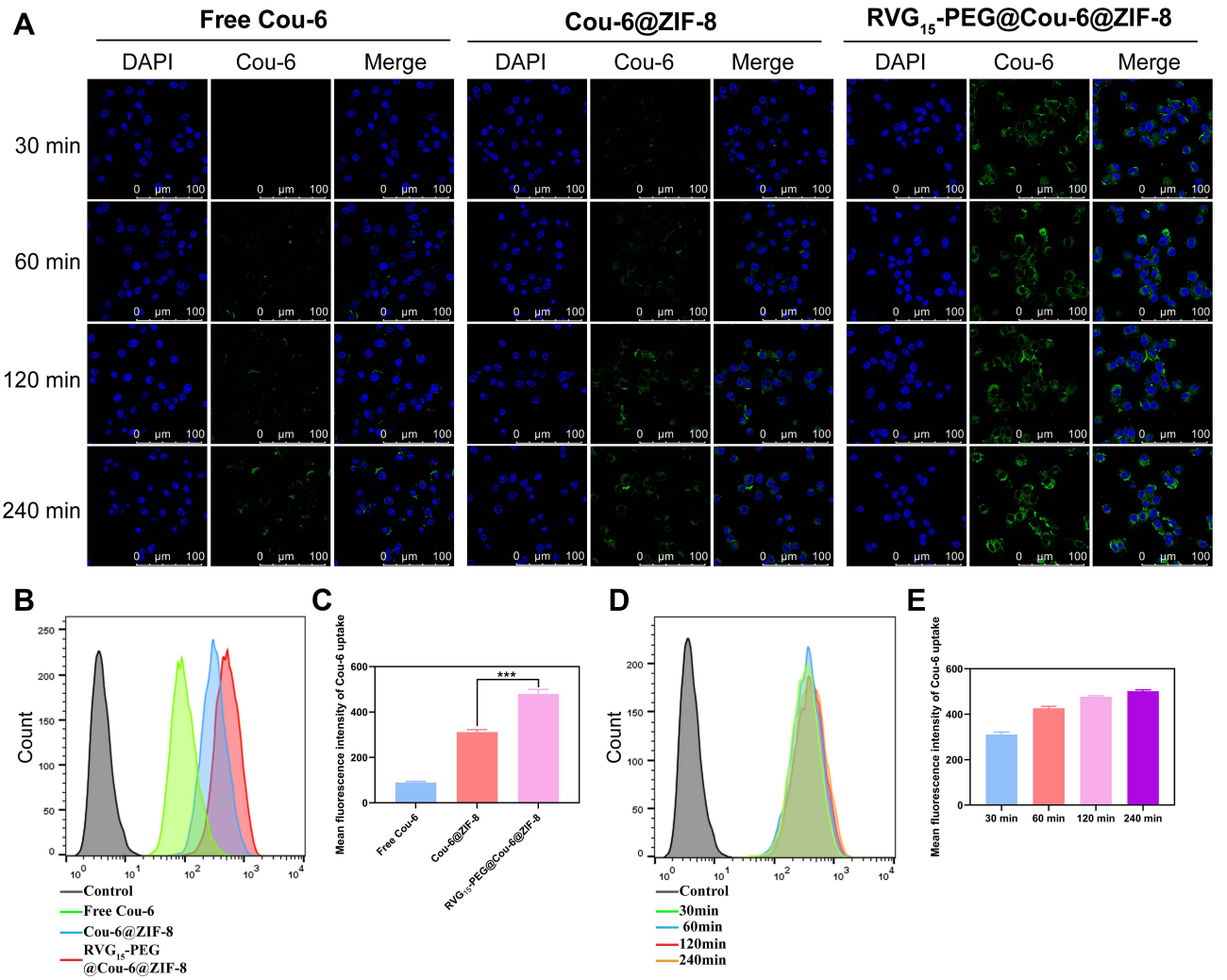

Figure 3 In vitro cellular uptake on HBMEC cells. (**A**) CLSM observation of HBMEC cells after treatment with free Cou-6, Cou-6@ZIF-8, and RVG_{15}-PEG@Cou-6@ZIF-8 for 30, 60, 120, and 240 min. (**B** and **C**) Quantitative analysis of cellular uptake by flow cytometry after incubation with free Cou-6, Cou-6@ZIF-8, and RVG_{15}-PEG@Cou-6@ZIF-8 for 1 h, respectively. Means ± SD, n = 3; ***P < 0.001. (**D** and **E**) Quantitative analysis of cellular uptake by flow cytometry after incubation with RVG_{15}-PEG@Cou-6@ZIF-8 for 30, 60, 120, and 240 min. Green: coumarin-6, blue: DAPI (nuclei).

intensity of approximately 47.0%, implying that the endocytosis of RVG_{15}-modified nanoparticles was more strongly mediated by caveolae proteins. After treatment with sodium azide, CPZ, and Col. RVG_{15}-PEG@Cou-6@ZIF-8 also showed decreased cellular uptake, with fluorescence intensities of 78.2%, 80.5%, and 76.0%, respectively. This result suggests that energy-dependent endocytosis, clathrin-mediated endocytosis, and microtubule-mediated endocytosis may be involved in the cellular uptake pathway of RVG_{15}-modified nanoparticles. As shown in Figure S3, 4T1 cells with low nAChR-expression showed reduced uptake compared with HBMECs and C6 cells. Finally, uptake reduced in HBMECs and C6 cells after pre-incubation with an excess of RVG_{15}. These results suggest that RVG_{15}-PEG@DTX@ZIF-8 crosses the BBB and enters tumor cells through nAChR receptor-mediated endocytosis.

C6 and HBMECs Cells Viability Assay

Inspired by the appreciable cellular uptake of RVG_{15}-modified nanoparticles, we further explored the relevant anti-tumor effect in vitro using the CCK-8 assay. First, the in vitro cytotoxicity of the blank ZIF-8 was measured. As shown in Figure 5A and Figure 5B, blank ZIF-8 exhibited negligible cytotoxicity in both HBMECs and C6 cells after 24 or 48 h of incubation, where the viability was greater than 85% at all tested concentrations. Thus, blank ZIF-8 is safe and biocompatible for further in vivo biomedical applications. Subsequently, the CCK-8 assay was used to assess the cytotoxicity of the as-prepared nanoparticles on C6 cells after incubation for 24 or 48 h. As shown in Figure 5C and

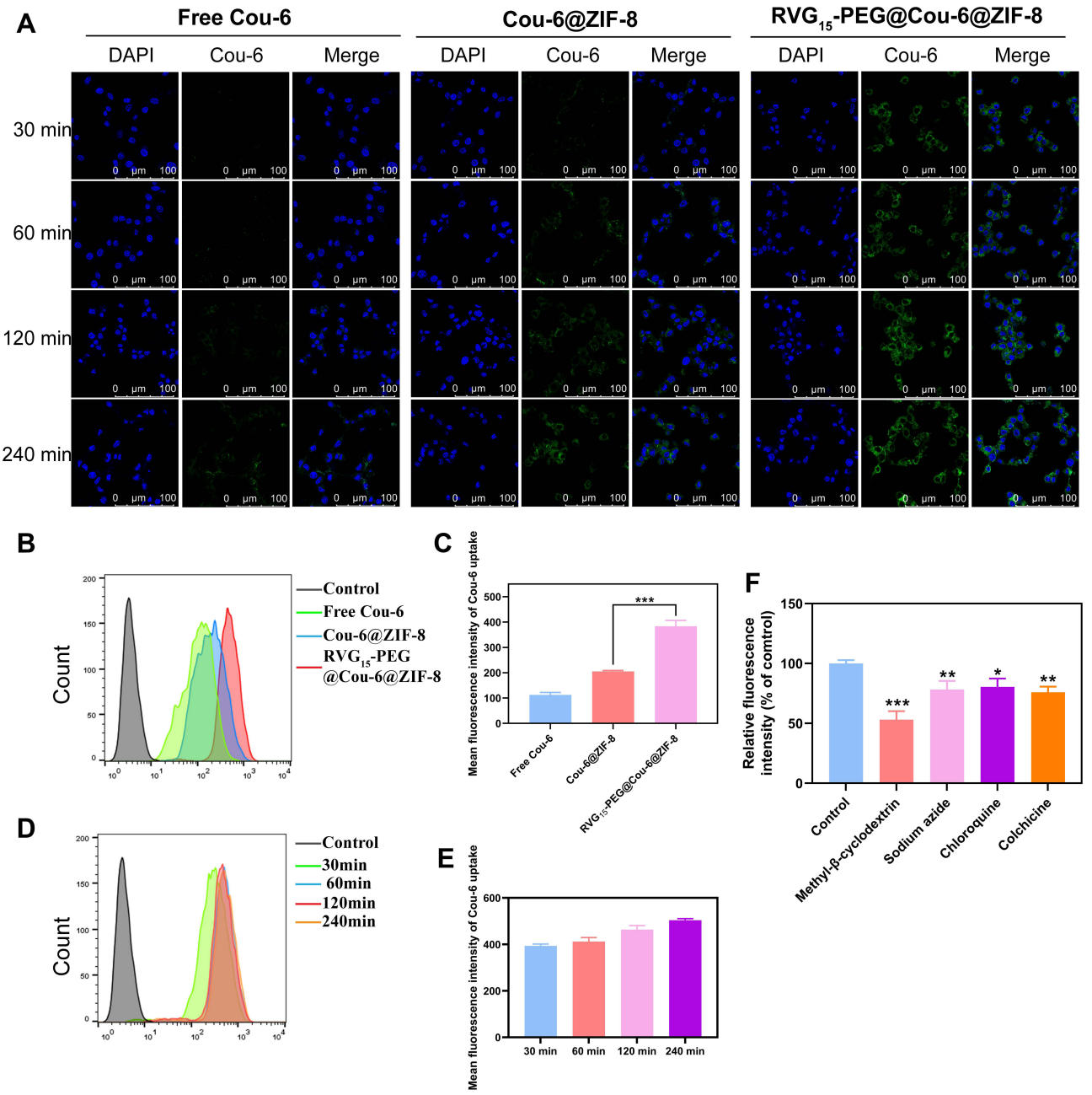

Figure 4 In vitro cellular uptake in C6 cells. (**A**) CLSM observation of C6 cells after treatment with free Cou-6, Cou-6@ZIF-8, and RVG_{15}-PEG@Cou-6@ZIF-8 for 30, 60, 120, and 240 min. (**B** and **C**) Quantitative analysis of cellular uptake by flow cytometry after incubation with free Cou-6, Cou-6@ZIF-8, and RVG_{15}-PEG@Cou-6@ZIF-8 for 1 h, respectively. Means ± SD, n = 3; ***P < 0.001. (**D** and **E**) Quantitative analysis of cellular uptake by flow cytometry after incubation with RVG_{15}-PEG@Cou-6@ZIF-8 for 30, 60, 120, and 240 min. (**F**) Cellular uptake analysis of RVG_{15}-PEG@Cou-6@ZIF-8 after incubation with different endocytic inhibitors by flow cytometry. Green: coumarin-6, blue: DAPI (nuclei). Means ± SD, n = 3; *P < 0.05, **P < 0.01, ***P < 0.001.

Figure 5D, free DTX, DTX@ZIF-8, and RVG_{15}-PEG@DTX@ZIF-8 showed dose-dependent inhibitory effects against C6 cell proliferation. Notably, RVG_{15}-PEG@DTX@ZIF-8 showed the highest cytotoxicity toward C6 cells compared to free DTX and DTX@ZIF-8. After 24 h of incubation, the IC_{50} values of free DTX, DTX@ZIF-8, and RVG_{15}-PEG@DTX@ZIF-8 were 2.885, 0.8651, and 0.09142 μg/mL, respectively. The corresponding IC_{50} values were 0.6538, 0.1037, and 0.02081 μg/mL, respectively, when the incubation time was extended to 48 h. The significantly

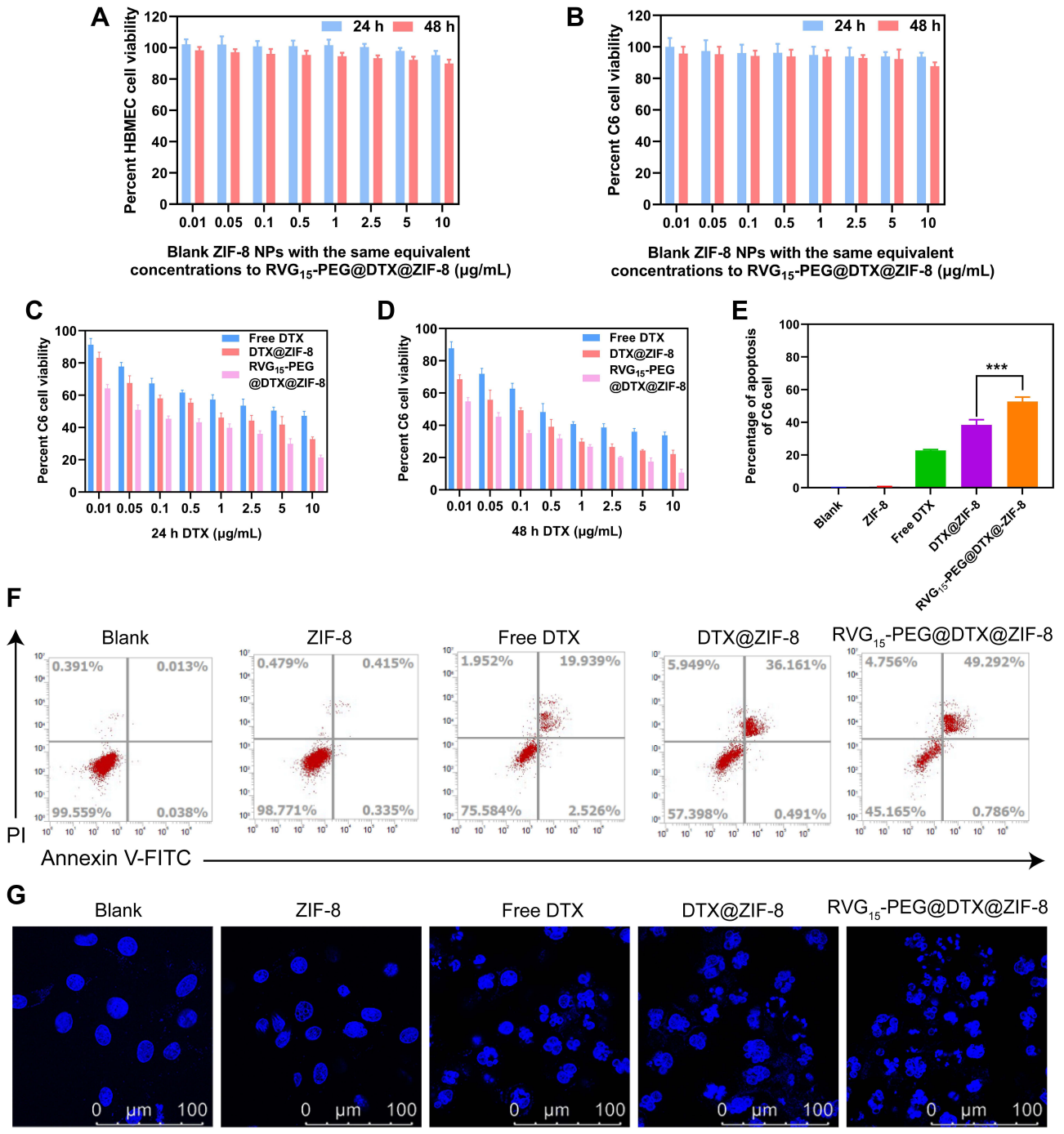

Figure 5 In vitro cytotoxicity and cell apoptosis study. In vitro cytotoxicity and cell apoptosis of blank ZIF-8, free DTX, DTX@ZIF-8, and RVG_{15}-PEG@DTX@ZIF-8 on C6 cells. (**A**) In vitro cytotoxicity of blank ZIF-8 on HBMEC cells after incubation for 24 and 48 h. (**B**) In vitro cytotoxicity of blank ZIF-8 on C6 cells after incubation for 24 and 48 h. (**C** and **D**) Inhibitory capacity of free DTX, DTX@ZIF-8, and RVG_{15}-PEG@DTX@ZIF-8 against C6 cell proliferation. (**E** and **F**) Flow cytometry results of C6 cell apoptosis and the percentage of early and late apoptosis after 24 h of treatment with blank ZIF-8, free DTX, DTX@ZIF-8, and RVG_{15}-PEG@DTX@ZIF-8 (n = 3, Means ± SD), ***P < 0.001. (**G**) CLSM images of C6 cells with Hoechst staining after 24 h of incubation with blank ZIF-8, free DTX, DTX@ZIF-8, and RVG_{15}-PEG@DTX@ZIF-8.

enhanced anti-proliferative effect of RVG_{15}-PEG@DTX@ZIF-8 might be due to the higher cellular internalization of nanoparticles based on RVG_{15} binding to nAChR on the surface of C6 cells. Taken together, these results suggest that RVG_{15}-PEG@DTX@ZIF-8 exerts strong cytotoxicity and may have a better curative effect on tumors in vivo.

C6 Cell Apoptosis Assay

Flow cytometry and CLSM analyses were performed to evaluate C6 cell apoptosis induced by blank ZIF-8, free DTX, DTX@ZIF-8, and RVG15-PEG@DTX@ZIF-8 (DTX concentration of 0.5 μg/mL), with complete culture medium as the control. Figure 5E and F show that the percentage of cells in the early and late apoptosis stages was 52.7% after 24 h incubation with RVG_{15}-PEG@DTX@ZIF-8, which was significantly higher than 0.6%, 22.8%, and 38.5% for blank ZIF-8, free DTX, and DTX@ZIF-8, respectively. These results indicated that RVG_{15}-PEG@DTX@ZIF-8 treatment notably induced cell apoptosis compared to the other treatments, which might be attributed to the higher uptake of RVG_{15}-PEG@DTX@ZIF-8 by C6 cells and its higher effectiveness in inducing tumor cell apoptosis. Blank ZIF-8 had little effect on C6 cell apoptosis. Furthermore, similar results were observed using CLSM. As shown in Figure 5G, the nuclei of the C6 cells in the control group were spherical and integral after Hoechst staining. The nuclei of the C6 cells cultured with blank ZIF-8 were not impaired, suggesting the safety of blank ZIF-8 for C6 cells. The nuclei of cells incubated with free DTX and DTX@ZIF-8 were moderately damaged. The nuclei of C6 cells were severely fragmented upon exposure to RVG_{15}-PEG@DTX@ZIF-8, suggesting that the nuclei were condensed and distributed into apoptotic bodies.

In vitro Wound-Healing Assay

To further investigate the antimetastatic effect of RVG_{15}-PEG@DTX@ZIF-8, a wound-healing assay was used to evaluate random cell migration and invasion. As shown in Figure 6, scratches in the blank group healed gradually. After treatment with free DTX, DTX@ZIF-8, or RVG_{15}-PEG@DTX@ZIF-8, the morphology of C6 tumor cells became irregular, and the scratches remained clearly visible. These results indicated that DTX significantly inhibited C6 cell migration, thus distinctly reducing the degree of wound healing. However, scratches in the RVG_{15}-PEG@DTX@ZIF-8 group remained clearly visible owing to the greater cytotoxicity and distinct inhibition of C6 cell migration compared to the other groups. Importantly, RVG_{15}-PEG@DTX@ZIF-8 exhibited a stronger antimetastatic effect than the other formulations. The antimetastatic effect of RVG_{15}-PEG@DTX@ZIF-8 was attributed to the high cellular internalization in C6 tumor cells via nAChR-mediated transcytosis.

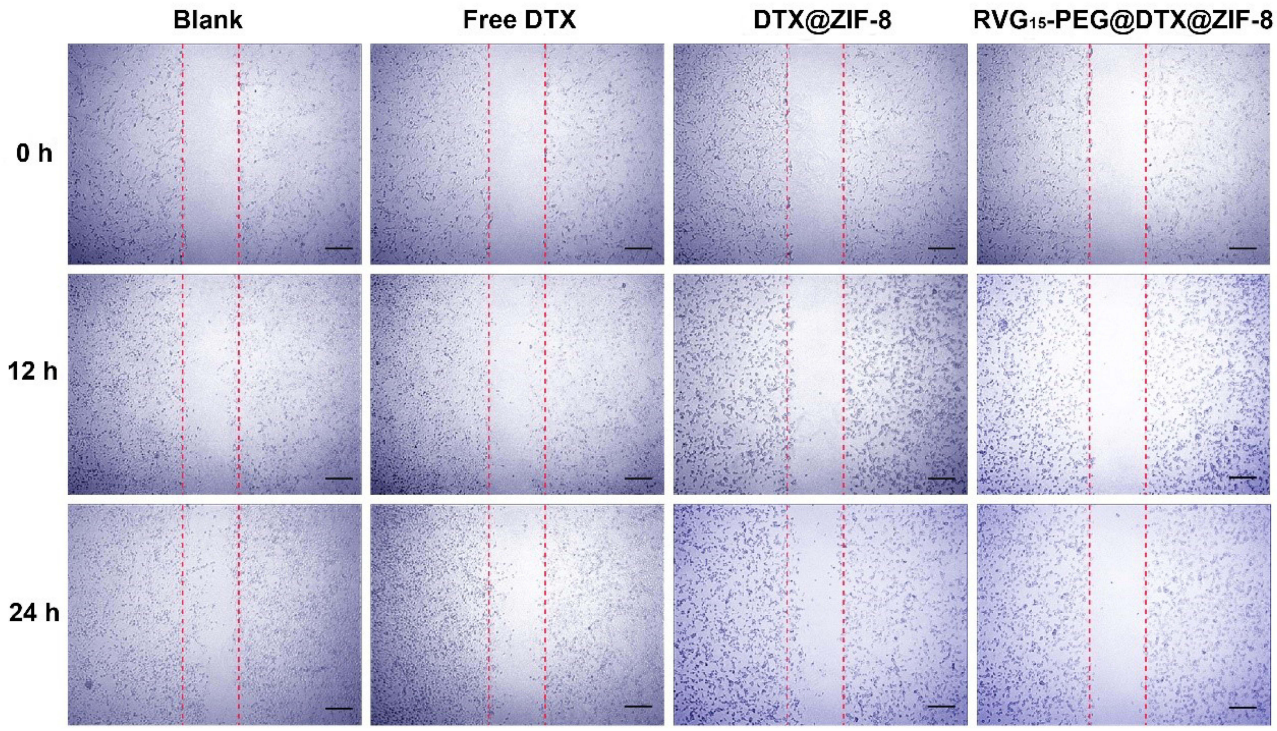

Figure 6 Wound healing assay on C6 cells. The images were captured at 0, 12, and 24 h. Scale bar = 100 μm.

In vitro Drug Penetration in the Blood–Brain Barrier Model

To screen and evaluate the potential of RVG_{15}-modified nanoparticles to cross the BBB, we used an in vitro BBB model in a dish. This model, based on co-cultures of either human or mouse endothelial cells and astrocytes on the two sides of a transwell membrane, accurately predicts the permeability of compounds and small molecules across the BBB.

More specifically, HBMECs and C6 cells were plated in the upper and lower chambers of the transwell system, respectively, to establish an in vitro BBB model (Figure 7A). A tightly bonded cell monolayer with a TEER above 200 $\Omega \cdot cm^2$ represents the successful formation of the in vitro BBB model. It has been reported that transporters and tight junction proteins expressed on this HBMEC cell monolayer are similar to those in BBB endothelial primary cells.[55,56] To clarify these results, the green fluorescent probe, Cou-6 was encapsulated into the nanoparticles, replacing DTX. The resulting nanoparticles were designated as Cou-6@ZIF-8 and RVG_{15}-PEG@Cou-6@ZIF-8. CLSM and flow cytometry were used to observe the BBB-penetrating abilities of the different nanoparticles in C6 cells in the lower chambers. As displayed in Figure 7B, free Cou-6 was blocked and hardly penetrated the BBB. Cou-6@ZIF-8 did not pass through the BBB monolayer. In contrast, RVG_{15}-PEG@Cou-6@ZIF-8 readily penetrated the BBB and was effectively taken up by the C6 cells in the lower chamber. Therefore, the intensity of green fluorescence in the cytoplasm was significantly higher. According to the quantitative results of flow cytometry (Figure 7C), the transport efficiency of RVG_{15}-PEG@Cou-6@ZIF-8 was 6.82- and 3.16-fold higher than that of free Cou-6 and Cou-6@ZIF-8. The results above validated the reliable capability of RVG_{15}-modified ZIF-8 nanoparticles in improving intracellular transduction and BBB penetration via nAChR-mediated transcytosis. High BBB permeation may facilitate the diffusion of therapeutic agents from the bloodstream into the brain in vivo, resulting in excellent antitumor effects in vivo.

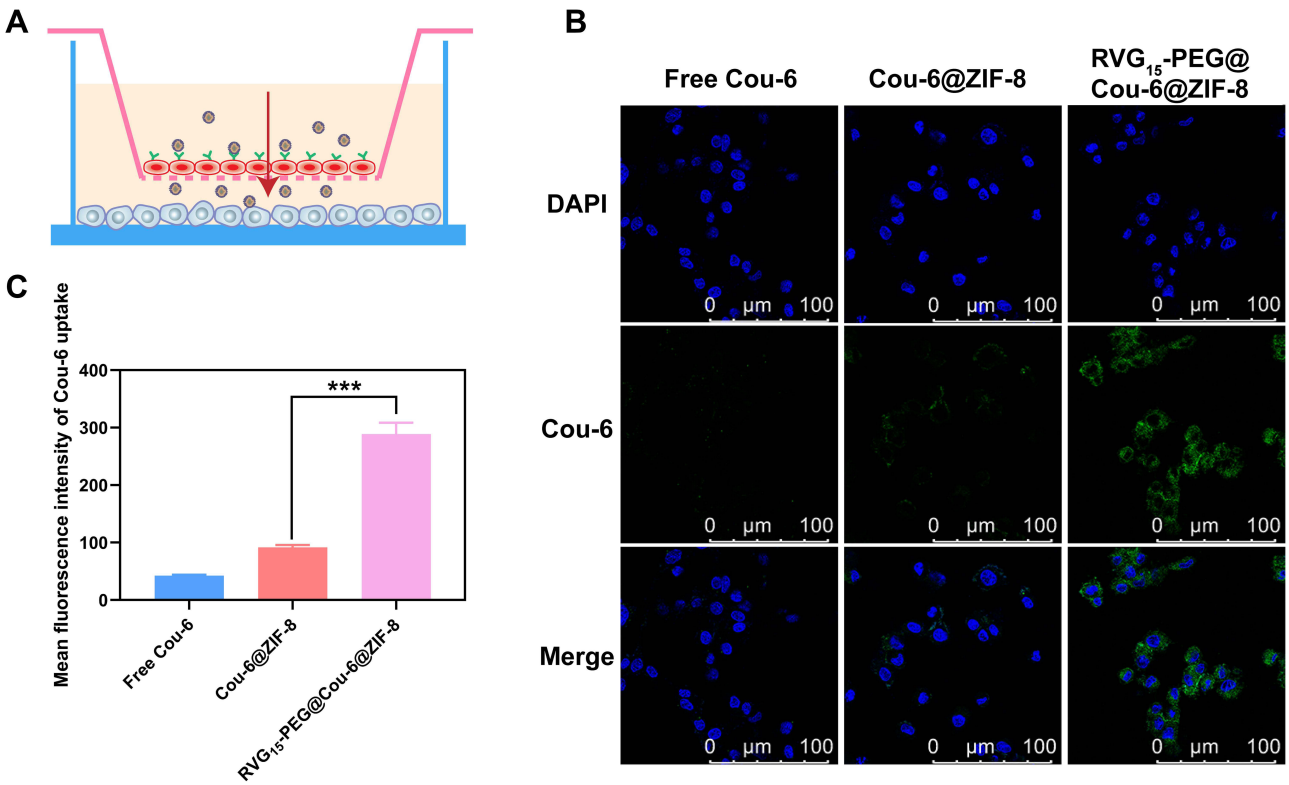

Figure 7 In vitro BBB permeation study. (**A**) Schematic diagram of the in vitro BBB model established by co-cultured HBMECs and C6 cells into the upper and lower chambers of a Transwell system. (**B**) CLSM analysis of uptake by C6 cells in the lower chamber after 2 h of incubation with free Cou-6, Cou-6@ZIF-8, and RVG_{15}-PEG@Cou-6@ZIF-8 in the upper chamber. (**C**) Quantitative analysis of uptake by C6 cells in the lower chamber by flow cytometry after incubation with free Cou-6, Cou-6@ZIF-8, and RVG_{15}-PEG@Cou-6@ZIF-8 for 2 h, respectively. Means ± SD, n = 3; ***P < 0.001.

In vivo Nanosystem Biodistribution

An essential prerequisite for satisfactory antitumor efficiency is that therapeutic agents can penetrate the BBB and accumulate in the tumor tissue at an effective concentration. Therefore, we systematically explored the biodistribution

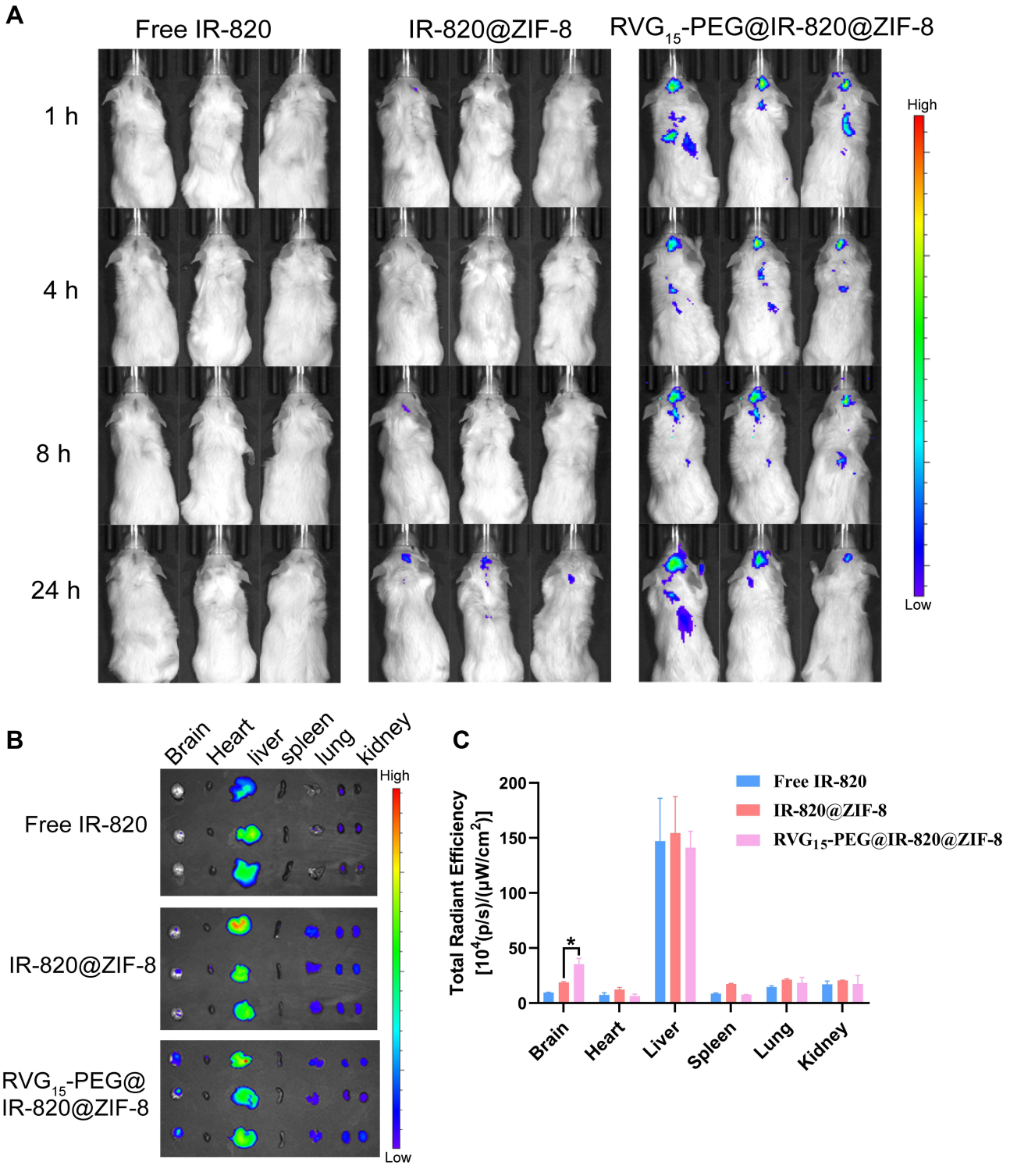

Figure 8 Biodistribution of free IR-820, IR-820@ZIF-8, and RVG_{15}-PEG@IR-820@ZIF-8 in vivo. (**A**) In vivo fluorescence imaging of orthotopic glioma-bearing mice treated with free IR-820, IR-820@ZIF-8, and RVG_{15}-PEG@IR-820@ZIF-8 at 1, 4, 8, and 24 h. (**B**) Ex vivo fluorescence images of the excised brains and major organs at 24 h after injection. (**C**) Quantitative region-of-interest analysis of (**B**). Means ± SD, n = 3; *P < 0.05.

and brain accumulation of RVG_{15}-modified ZIF-8 nanoparticles following systemic administration. Replacing DTX, the near-infrared dye IR-820 was encapsulated in these nanoparticles (IR-820@ZIF-8 and RVG_{15}-PEG@IR-820@ZIF-8) given its strong fluorescence signal for easy observation in vivo. An orthotopic glioma mouse model was established and administered free IR-820, IR-820@ZIF-8, and RVG_{15}-PEG@IR-820@ZIF-8. The fluorescence distributions of tumor-bearing mice were observed using an in vivo imaging system at predetermined times (1, 4, 8, and 24 h). As displayed in Figure 8A, it was perspicuously found that free IR-820 exhibited significant accumulation in the liver and kidneys, but negligible distribution into the brain. Similarly, glioma-bearing mice treated with IR-820@ZIF-8 showed strong fluorescence signals in the liver and weak signals at tumor sites. As expected, RVG_{15}-PEG@IR-820@ZIF-8 exhibited stronger fluorescence intensity in the brain because of the enhanced BBB penetration and specific targeting ability toward glioma benefiting from the RVG peptide. In particular, the fluorescence intensities of the tumor regions reached a maximum at 1 h post-injection and were maintained for 24 h. Subsequently, the mice were sacrificed at 24 h after injection, and the major organs (brain, heart, liver, spleen, lung, and kidney) were removed. Figure 8B shows ex vivo organ imaging, demonstrating a similar trend to the results from the in vivo image. The brain fluorescence intensity of mice treated with RVG_{15}-PEG@IR-820@ZIF-8 was 3.72- and 1.88-fold higher than that of mice treated with free IR-820 and IR-820@ZIF-8, respectively (Figure 8C). Collectively, these results indicate that RVG_{15} has excellent BBB penetration and glioma-targeting ability. Moreover, RVG_{15}-modified ZIF-8 nanoparticles display prolonged circulation time in vivo, thereby improving the efficacy of drug permeability and residence time in the brain.

In vivo Glioma-Bearing Brain Biodistribution

To intuitively visualize the distribution of therapeutic agents in glioma regions, frozen sections from C6 glioma-bearing mice 3 h after injection were prepared and observed by CLSM. As shown in Figure 9, the green Cou-6 was encapsulated in nanoparticles for visualization, replacing DTX. The nuclei were stained with DAPI (blue). The Cou-6@ZIF-8 group showed a negligible green fluorescence signal in the glioma region because of poor BBB penetration and low targeting capacity. By contrast, RVG_{15}-PEG@Cou-6@ZIF-8 significantly penetrated the BBB and showed a higher distribution in gliomas. Therefore, it was confirmed that RVG_{15} modification could significantly facilitate the BBB penetration of nanoparticles, enhance their accumulation within tumors, and achieve deep penetration into the tumor parenchyma by

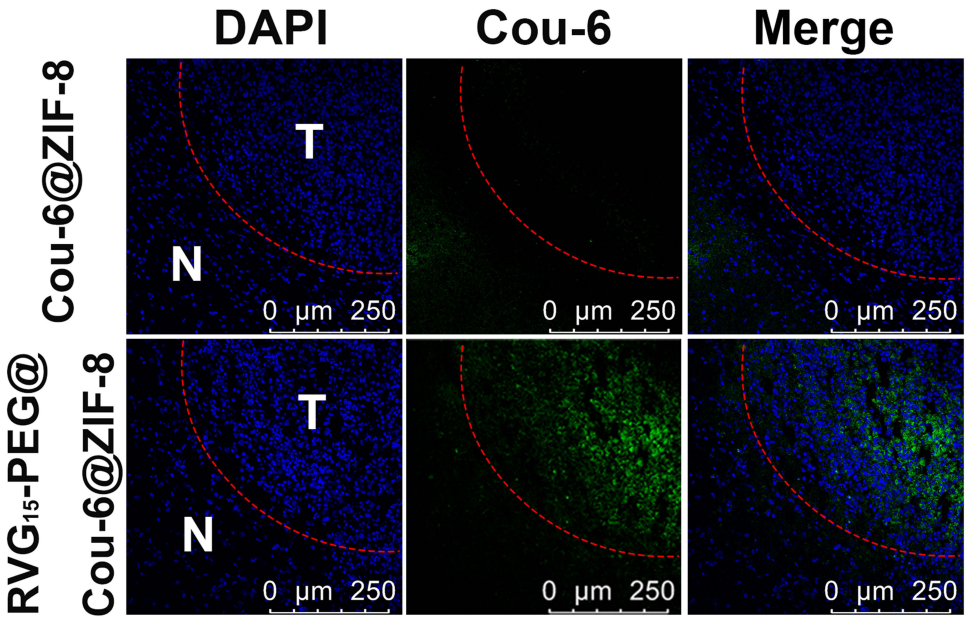

Figure 9 Tumor sections from C6 orthotopic glioma-bearing mice at 4 h following tail vein injection of Cou-6@ZIF-8 and RVG_{15}-PEG@Cou-6@ZIF-8. Blue, cell nuclei stained with DAPI; Green, Cou-6; N, normal brain sections; T, glioma section; Red line, boundary of the glioma.

nAChR-mediated transcytosis. The high capacity of RVG_{15}-modified ZIF-8 nanoparticles is expected to achieve effective antineoplastic effects in vivo.

In vivo Anti-Glioma Efficacy

Considering the potential of RVG_{15}-PEG@DTX@ZIF-8 as a brain-targeted and on-demand drug delivery system, its anti-glioma activity in vivo was investigated in C6 orthotopic implantation models. Glioma-bearing mice were randomly divided into four groups and intravenously injected with saline, free DTX, DTX@ZIF-8, or RVG_{15}-PEG@DTX@ZIF-8 at a dosage of 5 mg/kg DTX every 2 d (Figure 10A). The glioma was monitored by MRI. As shown in Figure 10B, the

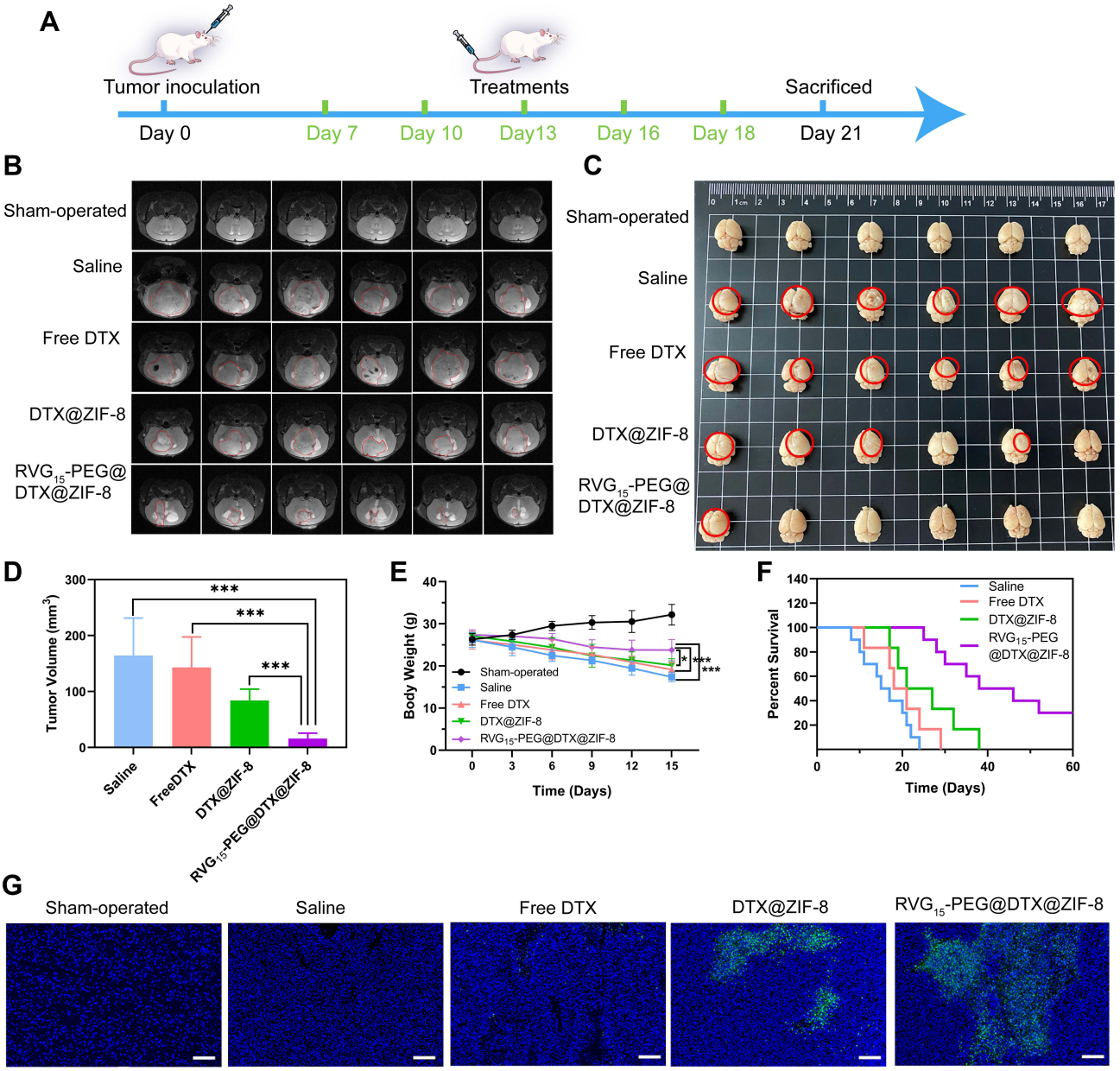

Figure 10 In vivo anti-glioma efficacy of RVG_{15}-PEG@DTX@ZIF-8 in C6 orthotopic glioma-bearing mice. (**A**) Schematic diagram of in vivo anti-glioma effect study. (**B**) MRI of brain in sham-operated group and brains from orthotopic glioma mice after treatment with saline, free DTX, DTX@ZIF-8, and RVG_{15}-PEG@DTX@ZIF-8. (**C**) Images of brain tissues isolated from orthotopic glioma mice after treatment with saline, free DTX, @DTX@ZIF-8, and RVG_{15}-PEG@DTX@ZIF-8. (**D**) Quantitative tumor volume analysis of (**B**). Means ± SD, n = 6; ***P < 0.001. (**E**) Body weight change of glioma tumor mice in the different groups at different time points. (n = 6). Means ± SD, n = 6; *P < 0.05, ***P < 0.001. (**F**) Kaplan–Meier survival curves of percentage survival of orthotopic glioma mice treated with saline, free DTX, DTX@ZIF-8, and RVG_{15}-PEG@DTX@ZIF-8, respectively (n = 10). (**G**) TUNEL assay of orthotopic glioma tumor tissues isolated from mice treated with saline, free DTX, DTX@ZIF-8, and RVG_{15}-PEG@DTX@ZIF-8 observed by CLSM. Green areas showed apoptosis of tumor cells. Scale bar = 200 μm.

sham-operated group showed little change in the structure of the brain. Free DTX and DTX@ZIF-8 exhibited weak anti-glioma effects. By contrast, the average glioma region of mice treated with RVG_{15}-PEG@DTX@ZIF-8 decreased significantly during the experiment. To further evaluate the anti-glioma effect of the nanoparticles, glioma regions in the brain, as examined by MRI, were quantified using the MRI software, as shown in Figure 10D. RVG_{15}-PEG@DTX@ZIF-8 displayed a stronger anti-glioma effect than free DTX or DTX@ZIF-8. On the third day after the final treatment, the mice were sacrificed, and brain tissues were collected and imaged (Figure 10C). Consistent with the above results, the tumor tissue of mice treated with RVG_{15}-PEG@DTX@ZIF-8 had a relatively smaller volume and less hemorrhage and necrosis (red circle). The superior anti-glioma activity of RVG_{15}-PEG@DTX@ZIF-8 was probably attributed to stronger BBB permeation, deeper glioma penetration, and higher cellular uptake via nAChR-mediated transcytosis. The systemic toxicity of the different formulations was investigated by monitoring the body weight of the mice every 3 days during the scheduled treatment period. Figure 10E shows a clear body weight change in mice treated with saline and free DTX, and the mice administered DTX@ZIF-8 showed moderate body weight loss. However, no obvious body weight loss was observed in mice treated with RVG_{15}-PEG@DTX@ZIF-8, indicating satisfactory safety.

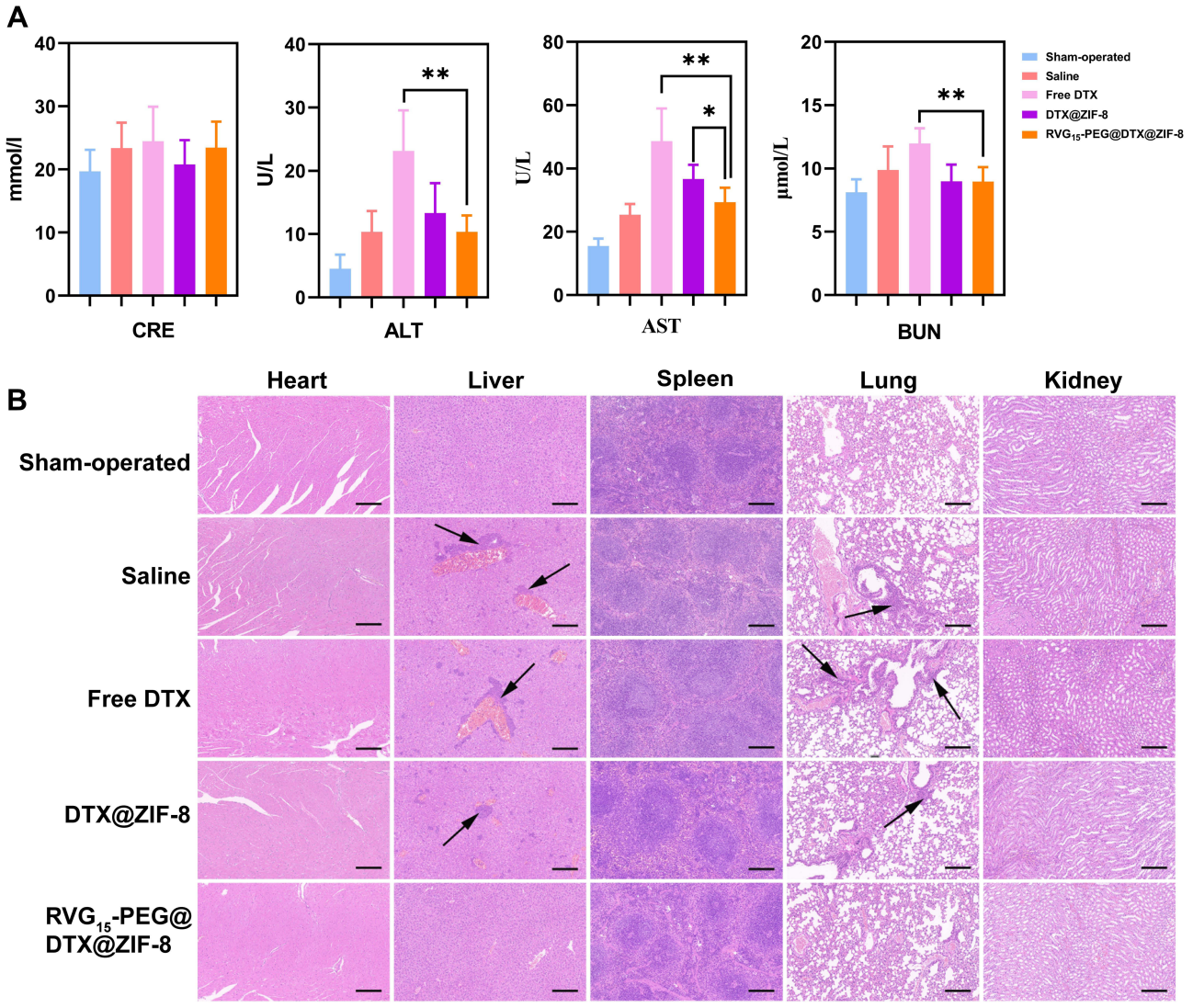

Figure 11 In vivo safety assessment and histological examination analysis. (**A**) CRE, ALT, AST, and BUN levels in blood samples isolated from orthotopic glioma tumor tissues after treatment with saline, free DTX, DTX@ZIF-8, and RVG_{15}-PEG@DTX@ZIF-8, respectively. Means ± SD, n = 6; *P < 0.05, **P < 0.01. (**B**) Hematoxylin and eosin staining of the hearts, livers, spleens, lungs, and kidneys after treatment with saline, free DTX, DTX@ZIF-8, and RVG_{15}-PEG@DTX@ZIF-8, as observed under an optical microscope. Scale bar = 200 μm.

Moreover, the TUNEL assay was employed to evaluate the antitumor efficacy and apoptosis of GBM cells. As shown in Figure 10G, the tumor tissue of mice treated with RVG_{15}-PEG@DTX@ZIF-8 revealed a stronger apoptosis level, with a large number of green TUNEL-positive cells. In comparison, the levels of apoptosis and necrosis in tumor tissue were apparently lower in both the free DTX and DTX@ZIF-8 groups. These results further demonstrate the potential of RVG_{15}-PEG@DTX@ZIF-8 as an effective therapeutic agent for treating gliomas.

Furthermore, the therapeutic efficacy of different treatments against GBM was investigated by plotting the median survival times. As shown in Figure 10F, the median survival times of saline, free DTX, and DTX@ZIF-8 groups were 16, 20, and 24 d, respectively. RVG_{15}-PEG@DTX@ZIF-8 prolonged the median survival time of C6-bearing mice to 42 days, which was significantly longer than that of the saline, free DTX, and DTX@ZIF-8 groups. These results demonstrated that RVG_{15}-PEG@DTX@ZIF-8 prolonged survival time in C6 orthotopic glioma-bearing mice.

Biocompatibility and Tissue Cytotoxicity in vivo

High biocompatibility and low tissue toxicity of the as-prepared RVG_{15}-modified ZIF-8 nanoparticles are essential for in vivo applications. Owing to the progression of glioma, the orthotopic GBM xenograft tumor model readily develops extensive lung and liver metastases. Therefore, we also investigated the antimetastatic capacity in the different treatment groups. At the end of treatment, the major organs (heart, liver, spleen, lungs, and kidneys) were collected and stained with hematoxylin and eosin. Pathological images are shown in Figure 11B. Metastasis and visible metastatic tumor nodules were observed in the excised lungs and liver of mice treated with saline, free DTX, and DTX@ZIF-8 (black arrow). However, mice treated with RVG_{15}-PEG@DTX@ZIF-8 displayed no abnormalities in any of the excised major organs, indicating that RVG_{15}-PEG@DTX@ZIF-8 significantly inhibited tumor metastasis. Thus, RVG_{15}-PEG@DTX@ZIF-8 can not only effectively inhibit in situ tumor growth but also completely suppress tumor metastasis. Furthermore, blood biochemical analyses, such as CRE, ALT, AST, and BUN, were analyzed. As shown in Figure 11A, the blood concentration levels of CRE, ALT, AST, and BUN remained negligible among all groups. Our results indicated the good biocompatibility and biosafety of the as-prepared RVG_{15}-modified MOF nanoparticles for in vivo drug delivery.

Conclusion

In this study, we developed RVG_{15}-based biomimetic MOF nanoparticles to promote the penetration of DTX to the BBB for GBM treatment. We demonstrated that this bionic nanotherapeutic system has excellent BBB permeability, enhanced brain endothelial and glioma cell selectivity, and improved tumor cell uptake due to surface modification by the RVG_{15} peptide. Simultaneously, we provide a simple and versatile strategy to decorate MOF nanoparticles with targeting ligands, whose mechanism is based on strong interactions between the metal ions of the MOF nanoparticles and the carboxyl group of the targeting ligand. However, we did not explore pharmacokinetic in depth, which is the focus of our future research.

Ethics Approval and Informed Consent

All animal experiments in this study were conducted in accordance with the protocols approved by the Laboratory Animal Ethics Committee of the Institute of Materia Medica in CAMS and PUMC. The operational process followed national and institutional principles and protocols for the care and use of experimental animals.

Acknowledgments

We acknowledge the support from the National Natural Science Foundation of China (82104106, 82073778), the Fundamental Research Foundation for the Central Universities (3332021044, China), and CAMS Innovation Fund for Medical Sciences (CIFMS) (2021-I2M-1-026, China).

Author Contributions

All authors made a significant contribution to the work reported, whether that is in the conception, study design, execution, acquisition of data, analysis and interpretation, or in all these areas; took part in drafting, revising or critically reviewing the article; gave final approval of the version to be published; have agreed on the journal to which the article has been submitted; and agree to be accountable for all aspects of the work.

Disclosure

The authors declare no conflicts of interest in this work.

References

1. Sung H, Ferlay J, Siegel RL, et al. Global cancer statistics 2020: globocan estimates of incidence and mortality worldwide for 36 cancers in 185 countries. *CA Cancer J Clin*. 2021;71:209–249. doi:10.3322/caac.21660
2. Ruan H, Chai Z, Shen Q, et al. A novel peptide ligand RAP12 of LRP1 for glioma targeted drug delivery. *J Control Release*. 2018;279:306–315. doi:10.1016/j.jconrel.2018.04.035
3. Szopa W, Burley TA, Kramer-Marek G, et al. Diagnostic and therapeutic biomarkers in glioblastoma: current status and future perspectives. *Biomed Res Int*. 2017;2017:8013575. doi:10.1155/2017/8013575
4. Shi K, Long Y, Xu C, et al. Liposomes combined an integrin αvβ3-specific vector with pH-responsible cell-penetrating property for highly effective antiglioma therapy through the blood-brain barrier. *ACS Appl Mater Interfaces*. 2015;7(38):21442–21454. doi:10.1021/acsami.5b06429
5. Davis ME. Glioblastoma: overview of disease and treatment. *Clin J Oncol Nurs*. 2016;20(5):2–8. doi:10.1188/16.CJON.S1.2-8
6. Reni M, Mazza E, Zanon S, et al. Central nervous system gliomas. *Crit Rev Oncol Hematol*. 2017;113:213–234. doi:10.1016/j.critrevonc.2017.03.021
7. Kakwere H, Zhang H, Ingham ES, et al. Systemic immunotherapy with micellar resiquimod-polymer conjugates triggers a robust antitumor response in a breast cancer model. *Adv Healthc Mater*. 2021;10:e2100008. doi:10.1002/adhm.202100008
8. Chu X, Bu Y, Yang X. Recent research progress of chiral small molecular antitumor-targeted drugs approved by the FDA from 2011 to 2019. *Front Oncol*. 2021;11:785855. doi:10.3389/fonc.2021.785855
9. Dean AQ, Luo S, Twomey JD, et al. Targeting cancer with antibody-drug conjugates: promises and challenges. *MAbs*. 2021;13(1):1951427. doi:10.1080/19420862.2021.1951427
10. Li J, Chai Z, Lu J, et al. $\alpha_v\beta_3$-targeted liposomal drug delivery system with attenuated immunogenicity enabled by linear pentapeptide for glioma therapy. *J Control Release*. 2020;322:542–554. doi:10.1016/j.jconrel.2020.04.009
11. Aparicio-Blanco J, Romero IA, Male DK, et al. Cannabidiol enhances the passage of lipid nanocapsules across the blood-brain barrier both in vitro and in vivo. *Mol Pharm*. 2019;16:1999–2010. doi:10.1021/acs.molpharmaceut.8b01344
12. Pandit R, Chen L, Gotz J. The blood-brain barrier: physiology and strategies for drug delivery. *Adv Drug Deliv Rev*. 2020;165–166:1–14. doi:10.1016/j.addr.2019.11.009
13. Patel B, Yang PH, Kim AH. The effect of thermal therapy on the blood-brain barrier and blood-tumor barrier. *Int J Hyperthermia*. 2020;37(2):35–43. doi:10.1080/02656736.2020.1783461
14. Gu G, Gao X, Hu Q, et al. The influence of the penetrating peptide iRGD on the effect of paclitaxel-loaded MT1-AF7p-conjugated nanoparticles on glioma cells. *Biomaterials*. 2013;34(21):5138–5148. doi:10.1016/j.biomaterials.2013.03.036
15. Wang K, Zhang X, Liu Y, et al. Tumor penetrability and anti-angiogenesis using iRGD-mediated delivery of doxorubicin-polymer conjugates. *Biomaterials*. 2014;35(30):8735–8747. doi:10.1016/j.biomaterials.2014.06.042
16. Gandioso A, Cano M, Massaguer A, et al. A green light-triggerable rgd peptide for photocontrolled targeted drug delivery: synthesis and photolysis studies. *J Org Chem*. 2016;81(23):11556–11564. doi:10.1021/acs.joc.6b02415
17. Ruoslahti E. Tumor penetrating peptides for improved drug delivery. *Adv Drug Deliv Rev*. 2017;110–111:3–12. doi:10.1016/j.addr.2016.03.008
18. Ramsey JD, Flynn NH. Cell-penetrating peptides transport therapeutics into cells. *Pharmacol Ther*. 2015;154:78–86. doi:10.1016/j.pharmthera.2015.07.003
19. Chen Y-X, Wei CX, Lyu Y-Q, et al. Biomimetic drug-delivery systems for the management of brain diseases. *Biomater Sci*. 2020;8(4):1073–1088. doi:10.1039/C9BM01395D
20. Alyami MZ, Alsaiari SK, Li Y, et al. Cell-type-specific CRISPR/Cas9 delivery by biomimetic metal organic frameworks. *J Am Chem Soc*. 2020;142(4):1715–1720. doi:10.1021/jacs.9b11638
21. Schnell MJ, McGettigan JP, Wirblich C, et al. The cell biology of rabies virus: using stealth to reach the brain. *Nat Rev Microbiol*. 2010;8(1):51–61. doi:10.1038/nrmicro2260
22. Alvarez-Erviti L, Seow Y, Yin H, et al. Delivery of siRNA to the mouse brain by systemic injection of targeted exosomes. *Nat Biotechnol*. 2011;29(4):341–345. doi:10.1038/nbt.1807
23. Lafon M. Rabies virus receptors. *J Neurovirol*. 2005;11(1):82–87. doi:10.1080/13550280590900427
24. Villa-Cedillo SA, Rodriguez-Rocha H, Zavala-Flores LM, et al. Asn194Lys mutation in RVG29 peptide increases GFP transgene delivery by endocytosis to neuroblastoma and astrocyte cells. *J Pharm Pharmacol*. 2017;69(10):1352–1363. doi:10.1111/jphp.12766
25. Liu Y, Huang R, Han L, et al. Brain-targeting gene delivery and cellular internalization mechanisms for modified rabies virus glycoprotein RVG29 nanoparticles. *Biomaterials*. 2009;30(25):4195–4202. doi:10.1016/j.biomaterials.2009.02.051
26. Li X, Li S, Ma C, et al. Preparation of baicalin-loaded ligand-modified nanoparticles for nose-to-brain delivery for neuroprotection in cerebral ischemia. *Drug Deliv*. 2022;29(1):1282–1298. doi:10.1080/10717544.2022.2064564
27. Ouyang Q, Liu K, Zhu Q, et al. Brain-penetration and neuron-targeting DNA nanoflowers co-delivering miR-124 and rutin for synergistic therapy of Alzheimer's disease. *Small*. 2022;18(14):e2107534. doi:10.1002/smll.202107534
28. Pinheiro RGR, Granja A, Loureiro JA, et al. RVG29-functionalized lipid nanoparticles for quercetin brain delivery and Alzheimer's disease. *Pharm Res*. 2020;37(7):139. doi:10.1007/s11095-020-02865-1
29. Xie J, Shen Z, Anraku Y, et al. Nanomaterial-based blood-brain-barrier (BBB) crossing strategies. *Biomaterials*. 2019;224:119491. doi:10.1016/j.biomaterials.2019.119491
30. Reddy S, Tatiparti K, Sau S, et al. Recent advances in nano delivery systems for blood-brain barrier (BBB) penetration and targeting of brain tumors. *Drug Discov Today*. 2021;26(8):1944–1952. doi:10.1016/j.drudis.2021.04.008
31. Liu Y, Wang W, Zhang D, et al. Brain co-delivery of first-line chemotherapy drug and epigenetic bromodomain inhibitor for multidimensional enhanced synergistic glioblastoma therapy. *Exploration*. 2022;2(4):20210274. doi:10.1002/EXP.20210274
32. He W, Li X, Morsch M, et al. Brain-targeted codelivery of Bcl-2/Bcl-xl and Mcl-1 inhibitors by biomimetic nanoparticles for orthotopic glioblastoma therapy. *ACS Nano*. 2022;16(4):6293–6308. doi:10.1021/acsnano.2c00320

33. Ismail M, Yang W, Li Y, et al. Biomimetic Dp44mT-nanoparticles selectively induce apoptosis in Cu-loaded glioblastoma resulting in potent growth inhibition. *Biomaterials*. 2022;289:121760. doi:10.1016/j.biomaterials.2022.121760
34. Ivask A, Pilkington EH, Blin T, et al. Uptake and transcytosis of functionalized superparamagnetic iron oxide nanoparticles in an in vitro blood brain barrier model. *Biomater Sci*. 2018;6(2):314–323. doi:10.1039/C7BM01012E
35. Joh DY, Sun L, Stangl M, et al. Selective targeting of brain tumors with gold nanoparticle-induced radiosensitization. *PLoS One*. 2013;8(4):e62425. doi:10.1371/journal.pone.0062425
36. Lim WQ, Phua SZF, Xu HV, et al. Recent advances in multifunctional silica-based hybrid nanocarriers for bioimaging and cancer therapy. *Nanoscale*. 2016;8(25):12510–12519. doi:10.1039/C5NR07853A
37. Cao J, Li X, Tian H. Metal-organic framework (MOF)-based drug delivery. *Curr Med Chem*. 2020;27(35):5949–5969. doi:10.2174/0929867326666190618152518
38. Wu MX, Yang YW. Metal-organic framework (MOF)-based drug/cargo delivery and cancer therapy. *Adv Mater*. 2017;29(23):1606134. doi:10.1002/adma.201606134
39. Zhang C, Hong S, Liu MD, et al. pH-sensitive MOF integrated with glucose oxidase for glucose-responsive insulin delivery. *J Control Release*. 2020;320:159–167. doi:10.1016/j.jconrel.2020.01.038
40. Gandara-Loe J, Souza BE, Missyul A, et al. MOF-based polymeric nanocomposite films as potential materials for drug delivery devices in ocular therapeutics. *ACS Appl Mater Interfaces*. 2020;12(27):30189–30197. doi:10.1021/acsami.0c07517
41. Yao S, Wang Y, Chi J, et al. Porous MOF microneedle array patch with photothermal responsive nitric oxide delivery for wound healing. *Adv Sci*. 2022;9(3):e2103449. doi:10.1002/advs.202103449
42. Abdelhamid HN. Zeolitic imidazolate frameworks (ZIF-8) for biomedical applications: a review. *Curr Med Chem*. 2021;28(34):7023–7075. doi:10.2174/0929867328666210608143703
43. Wang Q, Sun Y, Li S, et al. Synthesis and modification of ZIF-8 and its application in drug delivery and tumor therapy. *RSC Adv*. 2020;10(62):37600–37620. doi:10.1039/D0RA07950B
44. Mi X, Hu M, Dong M, et al. Folic acid decorated zeolitic imidazolate framework (ZIF-8) loaded with baicalin as a nano-drug delivery system for breast cancer therapy. *Int J Nanomedicine*. 2021;16:8337–8352. doi:10.2147/IJN.S340764
45. Xu M, Hu Y, Ding W, et al. Rationally designed rapamycin-encapsulated ZIF-8 nanosystem for overcoming chemotherapy resistance. *Biomaterials*. 2020;258:120308. doi:10.1016/j.biomaterials.2020.120308
46. Lin Y, Zhong Y, Chen Y, et al. Ligand-modified erythrocyte membrane-cloaked metal-organic framework nanoparticles for targeted antitumor therapy. *Mol Pharm*. 2020;17:3328–3341. doi:10.1021/acs.molpharmaceut.0c00421
47. Dutta S. Immunotherapy of tumors by tailored nano-zeolitic imidazolate framework protected biopharmaceuticals. *Biomater Sci*. 2021;9(19):6391–6402. doi:10.1039/D1BM01161H
48. Rezaei M, Abbasi A, Varshochian R, et al. NanoMIL-100(Fe) containing docetaxel for breast cancer therapy. *Artif Cells Nanomed Biotechnol*. 2018;46(7):1390–1401. doi:10.1080/21691401.2017.1369425
49. Grant DS, Williams TL, Zahaczewsky M, et al. Comparison of antiangiogenic activities using paclitaxel (taxol) and docetaxel (taxotere). *Int J Cancer*. 2003;104(1):121–129. doi:10.1002/ijc.10907
50. Sampath P, Rhines LD, DiMeco F, et al. Interstitial docetaxel (taxotere), carmustine and combined interstitial therapy: a novel treatment for experimental malignant glioma. *J Neurooncol*. 2006;80(1):9–17. doi:10.1007/s11060-006-9159-4
51. Chu XY, Huang W, Wang YL, et al. Improving antitumor outcomes for palliative intratumoral injection therapy through lecithin- chitosan nanoparticles loading paclitaxel- cholesterol complex. *Int J Nanomedicine*. 2019;14:689–705. doi:10.2147/IJN.S188667
52. Guo H, Liu L, Hu Q, et al. Mixed solvent method for improving the size uniformity and cargo-loading efficiency of zif-8 nanoparticles. *Langmuir*. 2021;37(33):10089–10099. doi:10.1021/acs.langmuir.1c01399
53. Pang X, Wang T, Jiang D, et al. Functionalized docetaxel-loaded lipid-based-nanosuspensions to enhance antitumor efficacy in vivo. *Int J Nanomedicine*. 2019;14:2543–2555. doi:10.2147/IJN.S191341
54. Belhadj Z, Ying M, Cao X, et al. Design of Y-shaped targeting material for liposome-based multifunctional glioblastoma-targeted drug delivery. *J Control Release*. 2017;255:132–141. doi:10.1016/j.jconrel.2017.04.006
55. Meng L, Chu X, Xing H, et al. Improving glioblastoma therapeutic outcomes via doxorubicin-loaded nanomicelles modified with borneol. *Int J Pharm*. 2019;567:118485. doi:10.1016/j.ijpharm.2019.118485
56. Srinivasan B, Kolli AR, Esch MB, et al. TEER measurement techniques for in vitro barrier model systems. *SLAS Technol*. 2015;20(2):107–126. doi:10.1177/2211068214561025
57. Zhang H, Li Q, Liu R, et al. A versatile prodrug strategy to in situ encapsulate drugs in mof nanocarriers: a case of cytarabine-ir820 prodrug encapsulated zif-8 toward chemo-photothermal therapy. *Adv Funct Mater*. 2018;28(35):1802830. doi:10.1002/adfm.201802830
58. Khalil IA, Kogure K, Akita H, et al. Uptake pathways and subsequent intracellular trafficking in nonviral gene delivery. *Pharmacol Rev*. 2006;58(1):32–45. doi:10.1124/pr.58.1.8